

1 **Global radiative effects of solid fuel cookstove aerosol emissions**

2 Yaoxian Huang^{1,a}, Nadine Unger², Trude Storelvmo³, Kandice Harper¹, Yiqi Zheng³, and Chris
3 Heyes⁴

4 ¹School of Forestry and Environmental Studies, Yale University, New Haven, CT 06511, USA

5 ²College of Engineering, Mathematics and Physical Sciences, University of Exeter, Exeter, EX4
6 4QE, UK

7 ³Department of Geology and Geophysics, Yale University, New Haven, CT 06511, USA

8 ⁴International Institute for Applied Systems Analysis, Laxenburg, Austria

9 ^anow at: Department of Climate and Space Sciences and Engineering, University of Michigan,
10 Ann Arbor, MI 48109, USA

11 *Correspondence to:* Yaoxian Huang (yaoxian.huang1@gmail.com)

12 **Abstract.** We apply the NCAR CAM5-Chem global aerosol-climate model to quantify the net
13 global radiative effects of black and organic carbon aerosols from global and Indian solid fuel
14 cookstove emissions for the year 2010. Our assessment accounts for the direct radiative effects,
15 changes to cloud albedo and lifetime (aerosol indirect effect, AIE), impacts on clouds via the
16 vertical temperature profile (semi-direct effect, SDE), and changes in the surface albedo of snow
17 and ice (surface albedo effect). In addition, we provide the first estimate of household solid fuel
18 black carbon emission effects on ice clouds. Anthropogenic emissions are from the IIASA GAINS
19 ECLIPSE V5a inventory. A global dataset of black carbon (BC) and organic aerosol (OA)
20 measurements from surface sites and aerosol optical depth (AOD) from AERONET is used to
21 evaluate the model skill. Compared with observations, the model successfully reproduces the
22 spatial patterns of atmospheric BC and OA concentrations, and agrees with measurements to
23 within a factor of 2. Globally, the simulated AOD agrees well with observations, with normalized
24 mean bias close to zero. However, the model tends to underestimate AOD over India and China
25 by $\sim 19 \pm 4\%$ but overestimate it over Africa by $\sim 25 \pm 11\%$ (\pm represents modeled temporal
26 standard deviations for $n=5$ run years). Without BC serving as ice nuclei (IN), global and Indian
27 solid fuel cookstove aerosol emissions have a net global cooling radiative effects of -141 ± 4 mW
28 m^{-2} and -12 ± 4 mW m^{-2} , respectively (\pm represents modeled temporal standard deviations for $n=5$
29 run years). The net radiative impacts are dominated by the AIE and SDE mechanisms, which

30 originate from enhanced cloud condensation nuclei concentrations for the formation of liquid and
31 mixed-phase clouds, and a suppression of convective transport of water vapor from the lower
32 troposphere to the upper troposphere/lower stratosphere that in turn leads to reduced ice cloud
33 formation. When BC is allowed to behave as a source of IN, the net global radiative impacts of the
34 global and Indian solid fuel cookstove emissions range from -275 to $+154$ mW m^{-2} and -33 to $+24$
35 mW m^{-2} , with globally averaged values -59 ± 215 and 0.3 ± 29 mW m^{-2} respectively. Here, the
36 uncertainty range is based on sensitivity simulations that alter the maximum freezing efficiency of
37 BC across a plausible range: 0.01, 0.05 and 0.1. BC-ice cloud interactions lead to substantial
38 increases in high cloud (< 500 hPa) fractions. Thus, the net sign of the impacts of carbonaceous
39 aerosols from solid fuel cookstoves on global climate (warming or cooling) remains ambiguous
40 until improved constraints on BC interactions with mixed-phase and ice clouds are available.

41 **1. Introduction**

42 Worldwide 2-3 billion people rely on solid fuels for the majority of their energy needs (Legros et
43 al., 2009). This household biomass combustion includes burning wood fuel, agricultural residues
44 and dung for cooking, heating and lighting. Emissions from household solid fuel combustion
45 include greenhouse gases (carbon dioxide and methane), black carbon (BC), organic carbon (OC),
46 and other trace gases (e.g., nitrogen oxides). Globally, BC from household solid fuel emissions
47 accounts for approximately 25% of the total anthropogenic BC emissions (Bond et al., 2013).
48 Among different types of cookstoves, advanced charcoal stoves show lowest BC emission factors,
49 followed by simple charcoal, advanced biomass, rocket and simple wood stoves, respectively
50 (Garland et al., 2017). India contains a large concentration of solid fuel-dependent households:
51 approximately 160 million households use solid fuels for cooking (Venkataraman et al., 2010). In
52 India, residential biofuel combustion represents the dominant energy sector and accounts for over
53 50% of the total source of BC and OC emissions (Klimont et al., 2009). India has a long history
54 of unsuccessful stove intervention programs that have sometimes focused on health benefits
55 (Hanbar and Karve, 2002; Kanagawa and Nakata, 2007; Kishore and Ramana, 2002). Despite
56 years of interventions, the vast majority of Indian households still rely on traditional stoves (Legros
57 et al., 2009). The possible scope for global climate co-benefits in future Indian cookstove
58 intervention programs warrants further examination and analysis of this region. BC-rich household
59 solid fuel emission plays an important role in affecting regional air quality (Archer-Nicholls et al.,

60 2016; Carter et al., 2016; Liu et al., 2016) and influencing global climate change (Bauer et al.,
61 2010; Butt et al., 2016; Venkataraman et al., 2005). The human health consequences of solid fuel
62 combustion are substantial (Archer-Nicholls et al., 2016; Ezzati and Kammen, 2002; Lelieveld et
63 al., 2015). Nearly 9% of the global burden of disease is attributable to exposure to household air
64 pollution from solid fuels, equivalent to 2.9 million premature deaths and 86 million disability
65 adjusted life years (DALYs) annually (GBD 2015 Risk Factors Collaborators, 2016). Half of the
66 world's population is exposed to indoor air pollution, mainly attributable to solid fuel usage for
67 household cooking and heating (Bonjour et al., 2013; Smith et al., 2014).

68 Carbonaceous aerosols from solid fuel combustion interact with the Earth's radiation budget
69 directly by absorbing and scattering solar radiation (direct radiative effect, DRE) and indirectly by
70 changing cloud albedo and lifetime (aerosol indirect effect, AIE), modifying the vertical
71 temperature profile (semi-direct effect, SDE), and changing the surface albedo over snow and ice
72 (surface albedo effect, SAE) (Boucher et al., 2013; Chung, 2005; Chylek and Wong, 1995; Ghan,
73 2013; Ghan et al., 2012; Myhre et al., 2013). Carbonaceous aerosols affect cloud albedo and
74 lifetimes (the AIE) by acting as cloud condensation nuclei (CCN) or ice nuclei (IN), thus
75 modifying cloud properties and changing the top-of-atmosphere (TOA) radiative fluxes
76 (Lohmann, 2002; Lohmann et al., 2000; Penner et al., 1992; Pierce et al., 2007; Spracklen et al.,
77 2011b). The net climatic effect of carbonaceous aerosols from household solid fuel combustion is
78 not well constrained and even the sign is uncertain (Bond et al., 2013). Bauer et al. (2010)
79 estimated that the net global radiative impact of residential biofuel carbonaceous aerosol emissions
80 is -130 mW m^{-2} . Kodros et al. (2015) have estimated that net DRE of solid fuel aerosol emissions
81 ranges from -20 to $+60 \text{ mWm}^{-2}$, AIE from -20 to $+10 \text{ mWm}^{-2}$, with uncertainties due to
82 assumptions of the aerosol emission masses, size distribution, aerosol optical properties and
83 mixing states. Butt et al. (2016) reported that the net DRE and AIE of aerosols from the residential
84 emission sector (including coal) ranged from -66 to $+21 \text{ mW m}^{-2}$, and from -52 to -16 mW m^{-2} ,
85 respectively. Their study did not include greenhouse gases. Moreover, neither of the latter two
86 studies consider the aerosol cloud-lifetime effect (second indirect effect), SDE and SAE. From the
87 perspective of policy-relevant country-level assessment of cookstove burning on global climate,
88 Lacey and Henze (2015) revealed that solid fuel cookstove aerosol emissions resulted in global air
89 surface temperature changes ranging from 0.28 K cooling to 0.16 K warming; Lacey et al. (2017)

90 further concluded that emissions reductions, including both aerosols and greenhouse gases, from
91 China, India and Ethiopia contributed the most to the global surface temperature changes by 2050.

92 None of the previous assessments have included BC-ice cloud interactions that can exert a large
93 influence on the atmospheric radiation balance. A recent study by Kulkarni et al. (2016) showed
94 that BC could act as IN, which was also shown by past lab and field findings (Cozic et al., 2008;
95 DeMott et al., 1999; Koehler et al., 2009). With BC as IN, Penner et al. (2009) estimated that the
96 total radiative forcing of anthropogenic and biomass BC emissions was -300 to -400 mW m^{-2} , with
97 IN parameterizations following Liu and Penner (2005) and Kärcher et al. (2006). Gettelman et al.
98 (2012) further concluded that AIE from BC emissions was -60 mW m^{-2} , with ice nucleation
99 parameterization following Barahona and Nenes (2009). Hence, a re-assessment of the global
100 climate change impacts of carbonaceous aerosol emissions from the solid fuel cookstove sector
101 that newly incorporates BC as IN is urgently needed.

102 Here, we employ a global aerosol-climate model to quantify the impacts of solid fuel cookstove
103 carbonaceous aerosol emissions globally and from India on global climate change. Sect. 2 presents
104 the Methods including the evaluation measurement data sets for BC, OA and aerosol optical depth
105 (AOD), the model description and experimental design. Sect. 3 details the results of the model
106 evaluation and the impacts of the global and Indian solid fuel cookstove emissions on the
107 atmospheric radiation budget and global climate. Discussion and summary are provided in Sect.
108 4.

109 **2. Methods**

110

111 **2.1 BC and OC evaluation measurement database**

112 Ground-based BC observations are from IMPROVE (the Interagency Monitoring of PROtected
113 Visual Environment, <http://vista.cira.colostate.edu/Improve/>) for the year 2010 over North
114 America (Malm et al., 1994), EMEP (the European Monitoring and Evaluation Programme,
115 <http://ebas.nilu.no>) for 2009-2013 over Europe, and sporadic measurement campaigns for China
116 and India. Elemental carbon (EC) concentrations are measured using Thermal Optical Reflectance
117 (TOR) (Chow et al., 1993, 2004; EMEP/MSC-W et al., 2014). Our measurement database
118 comprises a total of 152 sites from IMPROVE, 28 sites from EMEP, 35 sites for China, and 41
119 sites for India. The number of urban sites includes 8 from IMPROVE, 5 from EMEP, 17 for China,

120 and 23 for India. Here we define urban (including semi-urban) sites as the geographic locations of
121 the measured sites locating in a city, others as rural sites.

122 A global network of aerosol mass spectrometer (AMS) surface measurements for organic aerosol
123 (OA) for 2000-2008 are used to compare with model simulations (Spracklen et al., 2011a; Zhang
124 et al., 2007; Zheng et al., 2015). The AMS technique measures hydrocarbon-like OA (HOA),
125 oxygenated OA (OOA) and total OA (HOA + OOA). HOA is a surrogate for primary OA (POA)
126 emitted directly from fossil fuel and biomass burning, while OOA is a surrogate for secondary OA
127 (SOA). In this study, we compare monthly mean total OA with model simulated total OA (POA +
128 SOA). The majority of the AMS measurements in the surface concentration database were made
129 prior to 2005.

130 Ground-based AOD observations from AERONET (AErosol RObtic NETwork,
131 <https://aeronet.gsfc.nasa.gov>) during 1993-2016 are applied to examine model skill (Dubovikl and
132 King, 2000; Holben et al., 1998, 2001). A climatological AOD value averaged over 1993-2016 for
133 each site is used to compare with the model simulation. The AERONET version 2 level-2 product
134 is used in this study.

135 **2.2 NCAR CAM5-Chem global model description**

136 We apply the NCAR Community Atmosphere Model version 5.3 with chemistry (CAM5-Chem)
137 within the Community Earth System Model (CESM) version 1.2.2 (Emmons et al., 2010;
138 Lamarque et al., 2012; Tilmes et al., 2015). The oxidant-aerosol system is fully coupled in CAM5-
139 Chem. The horizontal resolution of CAM5-Chem is 0.9° latitude by 1.25° longitude, with 56
140 vertical levels from surface up to about 40 km. In the standard CAM5-Chem, aerosol
141 microphysical processes are represented using a 3-mode scheme (MAM3; aitken, accumulation
142 and coarse modes). MAM3 simulates both mass and number concentrations of aerosols. Aerosol
143 size distributions in each mode are assumed to be lognormal (Liu et al., 2012). The model treats
144 the effects of aerosol acting as CCN in liquid-phase clouds (Ghan et al., 2012). The aerosol
145 components in MAM3 include BC, primary organic matter (POM), secondary organic aerosol
146 (SOA), sulfate, sea salt and dust, which are assumed to be internally mixed within each lognormal
147 mode. Specifically, BC and POM from solid fuel cookstove emissions are treated in the
148 accumulation mode, with size range of 0.058-0.27 μm (Liu et al., 2012). Mass yields of semi-

149 volatile organic gas-phase species (SOAG) from emissions of isoprene, monoterpenes, big alkanes
150 and alkenes, as well as toluene are prescribed (Emmons et al., 2010; Liu et al., 2012; Tilmes et al.,
151 2015). The condensable SOAG reversibly and kinetically partitions into the aerosol phase to form
152 SOA in CAM5-Chem as described in Liu et al. (2012).

153 **2.3 Emissions**

154 Global anthropogenic emissions are from the IIASA (International Institute for Applied System
155 Analysis) Greenhouse Gas-Air Pollution Interactions and Synergies (GAINS) integrated
156 assessment model ECLIPSE V5a (Evaluating the Climate and Air Quality Impacts of Short-lived
157 Pollutants version 5a) for the year 2010 (Amann et al., 2011, 2013; Klimont et al., 2017; Stohl et
158 al., 2015). Species in ECLIPSE V5a include BC, POM, sulfur dioxide, nitrogen oxides, carbon
159 monoxide, volatile organic compounds, and ammonium, with their annual global budgets for the
160 year 2010 shown in Table 1. ECLIPSE V5a emissions available at 0.5° latitude by 0.5° longitude
161 spatial resolutions are re-gridded to the model spatial resolution. ECLIPSE V5a does not include
162 shipping or wildfire biomass burning emissions, which are instead obtained from the IPCC AR5
163 RCP8.5 scenario for the year 2010 (Riahi et al., 2011).

164 **2.4 Simulations: BC not active as IN**

165 Atmosphere-only simulations are performed in specified dynamics (SD) mode with offline
166 meteorological fields from the Goddard Earth Observing System model version 5 (GEOS-5). In
167 this SD mode configuration, the internally derived meteorological fields (e.g., horizontal wind
168 component, air temperature and latent heat flux) are nudged by 10% towards reanalysis fields from
169 GEOS-5 for every model time step. The nudging technique in CAM5-Chem has been evaluated to
170 quantify the aerosol indirect effect in order to reduce the influence of natural variability
171 (Kooperman et al., 2012). Sea surface temperature and sea ice in the model are prescribed from
172 the Climatological/Slab-Ocean Data Model (DOCN) and Climatological Ice Model (DICE)
173 respectively, with monthly-varying decadal mean averaged over 1981-2010.

174 We perform three sets of model simulations using the model configurations shown in Table 2. The
175 first set of simulations represents the control with anthropogenic emissions following ECLIPSE
176 V5a, as described above (hereafter referred to as BASE). The second set of simulations are

177 identical to the BASE simulation except the global solid fuel cookstove emissions for aerosols and
178 gas-phase aerosol and ozone precursors are set to zero (termed as GBLSF_OFF). The third set of
179 simulations is identical to BASE except the solid fuel cookstove emissions are set to zero over the
180 Indian sub-continent (termed as INDSF_OFF). We run all the above simulations for 6 years from
181 2005 to 2010, with the first year discarded as spin-up and the last five years averaged for output
182 analysis. The differences between BASE and GBLSF_OFF isolate the impacts of the global solid
183 fuel cookstove sector aerosol emissions, and the differences between BASE and INDSF_OFF
184 isolate the impacts of the Indian solid fuel cookstove sector aerosol emissions. Top-of-the-
185 atmosphere (TOA) aerosol shortwave (SW) and longwave (LW) radiative effects are calculated
186 using the Rapid Radiative Transfer Model for GCMs (RRTMG) that is coupled to CAM5-Chem
187 (Ghan, 2013; Ghan et al., 2012).

188 **2.5 Simulations: BC active as IN**

189 In default CAM5-Chem, BC is not treated as IN (Liu et al., 2012; Tilmes et al., 2015). IN
190 concentrations from homogeneous nucleation are calculated as a function of vertical velocity (Liu
191 et al., 2007). Several lab and field studies indicate that BC particles can act as IN (Cozic et al.,
192 2008; DeMott et al., 1999; Koehler et al., 2009; Kulkarni et al., 2016). Therefore, we conduct
193 additional simulations that treat BC as an effective IN applying the ice nucleation scheme of
194 Barahona and Nenes (2008, 2009). The scheme estimates maximum supersaturation and ice crystal
195 concentrations and considers competition between homogeneous and heterogeneous freezing.
196 Homogeneous nucleation occurs in solution droplets formed on soluble aerosols (mainly sulfate),
197 while heterogeneous nucleation occurs on IN, which here are a small subset of mineral dust and
198 black carbon particles. The heterogeneous freezing of BC and dust is described as a generalized
199 ice nucleation spectrum.

200 We perform three additional model simulations, with model configurations identical to those in
201 Table 2, except for the treatment of BC particles as effective IN. In addition, for each model
202 simulation, we alter the plausible maximum freezing efficiency (MFE) of BC as 0.01, 0.05 and 0.1
203 that provides an uncertainty range in the global climatic impact assessment.

204 **3 Results**

205 **3.1 Evaluation of surface BC and OA concentrations**

206 Surface observation networks from IMPROVE, EMEP, and various campaigns in China and India
207 are employed to compare with model simulations, as shown in Figure 1. We diagnose the
208 normalized mean bias (NMB) for each source region, calculated as

$$209 \quad \text{NMB} = \left(\frac{\sum_i (M_i - O_i)}{\sum_i O_i} \right) \times 100\% \quad (1)$$

210 where M and O represent monthly mean model simulated and observational concentrations at site
211 i respectively, and \sum is the sum over all the sites within a source region.

212 In general, the model simulated surface BC concentrations agree with observations to within a
213 factor of 2, consistent with previous studies (Huang et al., 2013; Wang et al., 2011, 2014a, 2014b).
214 A total of 41 surface BC observational sites are used to evaluate the model simulation over India
215 (Fig. 1a). On average, the model underestimates surface BC concentrations by approximately 45%
216 and 34% over urban and rural sites respectively, with a total NMB -41% (Fig. 1a), which implies
217 a marked underestimation of the BC emissions in India. Previous modeling studies have also
218 reported large underestimates of BC surface concentrations over India against observations
219 (Gadhavi et al., 2015; He et al., 2014; Zhang et al., 2015). Part of the model/measurement
220 discrepancy is related to a sampling bias because the majority of the observations are located over
221 urban or heavily polluted regions. For China sites, the NMB value is -16% (Fig. 1b). Similar to
222 India, the model substantially underestimates the surface BC concentrations over urban sites with
223 a NMB of -30%. However, the model performs relatively well over rural areas, with a NMB close
224 to zero. For IMPROVE, the NMB values for rural and urban sites are -15% and -43%, respectively,
225 with a total NMB -28% (Fig. 1c). Over Europe, the model simulated surface BC concentrations
226 agree quite well with observations, with a NMB value of -8%, although two urban sites show
227 substantial model underestimation (Fig. 1d).

228 The 40 AMS surface OA measurements are grouped into three categories: East Asia (8 sites),
229 North America (17 sites) and Europe (15 sites) (Spracklen et al., 2011a; Zhang et al., 2007; Zheng
230 et al., 2015). Figure 2 shows the evaluation of simulated surface OA against observations. Over
231 East Asia, the model slightly underestimates observed OA, with a NMB of $-8.5 \pm 5\%$ (\pm represents
232 modeled temporal standard deviations for $n=5$ run years) (Fig. 2a). In contrast, the simulated OA
233 concentrations overestimate the measurements by over a factor of 2 in North America, with a NMB

234 value of $124 \pm 24\%$ (Fig. 2b). For the European sites, we find a simulated OA overestimation of
235 measured concentrations by up to $0.9 \pm 0.7 \mu\text{g m}^{-3}$, corresponding to a NMB of $+32 \pm 26\%$ (Fig.
236 2c).

237 **3.2 Evaluation of model AOD**

238 Figure 3 compares simulated AOD values against observations over nine regions across the globe,
239 including India, China, Rest of Asia (excluding China and India), Africa, South America, North
240 America, Europe, Australia and remote regions. Over India, the simulated annual mean AOD is
241 lower than observations by about $16 \pm 3\%$ (Fig. 3a), with large bias sources mainly from the
242 northern India regions (e.g., New Delhi and Kanpur). This is consistent with Quennehen et al.
243 (2016) who also reported that model simulated AOD values were generally lower than satellite-
244 derived AOD over northern India, using the same emission inventory as our study. As discussed
245 in Sect. 3.1, model simulated surface BC concentrations over India are also underestimated (by up
246 to 41%), therefore, the low bias of model simulated AOD can be attributed, in part, to the
247 underestimation of Indian BC emissions from ECLIPSE V5a emission inventory (Stohl et al.,
248 2015), although global anthropogenic BC budgets in ECLIPSE V5a lie in the high end compared
249 with previous studies (Bond et al., 2004, 2013; Janssens-Maenhout et al., 2015). The model
250 underestimate of AOD from AERONET in India may also be related to the fairly coarse global
251 model resolution, as previously reported by Pan et al. (2015) and Zhang et al. (2015). A similar
252 pattern is found over China (Fig. 3b) and the rest of Asia (Fig. 3c), with NMB values of $-21 \pm 4\%$
253 and $-15 \pm 6\%$ respectively. Model simulated AOD values from several sites in West Asia (Fig. 3c)
254 are higher than observations, which is probably caused by the model overestimation of dust
255 emissions (He and Zhang, 2014). This directly leads to annual mean model simulated AOD values
256 over Africa $25 \pm 11\%$ higher than observations because Saharan dust emissions dominate the AOD
257 over North Africa (Fig. 3d). For South America, the model generally agrees quite well with
258 observations (Fig. 3e), except for a few sites where model simulated AOD values are lower than
259 observations by more than a factor of 2. This is probably due to the model underestimation of
260 biomass burning emissions there (Reddington et al., 2016). AOD values over North America (Fig.
261 3f) and Europe (Fig. 3g) are relatively lower (with values generally < 0.3), due to lower
262 anthropogenic emissions. In these two regions, modeled AOD agrees with observations within a
263 factor of 2, with NMB values $-20 \pm 4\%$ and $-18 \pm 9\%$ respectively. CAM5-Chem overestimates

264 AOD over Australia (Fig. 3h) and remote sites (Fig. 3i), with NMB values of $+69 \pm 17\%$ and $+47$
265 $\pm 12\%$, respectively. Globally, model simulated AOD agrees quite well with observations, with
266 NMB values close to zero.

267 **3.3 Contribution of solid fuel cookstove sector emissions to atmospheric BC and POM**

268 **3.3.1 BC**

269 Annual BC emissions and budgets are reported in Table 3 based on the anthropogenic inventory
270 from ECLIPSE V5a. Annual BC emissions from the global and Indian solid fuel cookstove
271 emissions are 2.31 and 0.36 Tg yr⁻¹, accounting for 23.7% and 3.7% of the total BC emissions. For
272 the control simulation, global annual mean BC burden and lifetime are 0.12 ± 0.001 Tg and $4.5 \pm$
273 0.04 days, respectively (Table 3), at the low end of the range estimated by AeroCom (Schulz et
274 al., 2006; Textor et al., 2006).

275 Figure 4 shows the zonal mean BC concentrations from the control simulation (Fig. 4a), global
276 (Fig. 4b) and Indian (Fig. 4c) solid fuel cookstove emissions respectively. For the control
277 simulation, in general, the highest BC concentrations (by up to $0.40 \mu\text{g m}^{-3}$) occur at the surface
278 over the emission source regions in the mid-latitudes (e.g., China and India). In the tropics and
279 mid-latitudes, zonal mean BC concentrations decrease with increasing altitude, due to wet removal
280 and deposition, as found in Huang et al. (2013). A similar vertical distribution is observed for the
281 impacts from global and Indian solid fuel cookstove emissions, although the magnitude is smaller,
282 compared with the control simulation. Annual mean BC burdens from global and Indian solid fuel
283 cookstove emissions account for about $24.2 \pm 0.7\%$ and $5.0 \pm 0.0\%$ of that in the control simulation
284 (0.12 ± 0.001 Tg).

285 **3.3.2 POM**

286 Global POM emissions are mainly from biomass burning (31 Tg yr⁻¹) and anthropogenic emissions
287 (18.9 Tg yr⁻¹), with global and Indian solid fuel cookstove emissions accounting for, 21% and
288 3.4% respectively, of the total POM emissions (Table 3). In our control simulation, the annual
289 mean POM burden is 0.66 ± 0.006 Tg, and the global annual mean POM lifetime is 4.8 ± 0.04
290 days (Table 3).

291 In Figure 5, we show the annual zonal mean POM concentrations for the control simulation (Fig.
292 5a) and for global (Fig. 5b) and Indian (Fig. 5c) solid fuel cookstove emissions. There are two
293 maxima in the annual zonal mean POM concentrations near the surface. One is located in the
294 tropics due to the large biomass burning emissions there, and the other is located over mid-latitude
295 regions and originates mainly from anthropogenic emissions (Chung and Seinfeld, 2002; Huang
296 et al., 2013). For POM concentrations from global solid fuel cookstove emissions, a single
297 maximum is evident in the Northern Hemisphere (NH) subtropics at the surface (Fig. 5b). The
298 surface maximum for the Indian solid fuel cookstove emissions reaches a maximum in the NH
299 subtropics. The annual mean POM burdens from global and Indian solid fuel cookstove emissions
300 are 0.13 ± 0.004 Tg and 0.027 ± 0.002 Tg respectively.

301 **3.4 Impacts of solid fuel cookstove aerosol emissions on global radiation budget**

302 **3.4.1 Direct radiative effect (DRE)**

304 The DRE impacts of the global and Indian solid fuel cookstove emissions are shown in Figure 6.
305 For the global solid fuel cookstove sector, the globally averaged DRE from aerosol emissions is
306 $+70 \pm 3$ mW m⁻² (\pm represents modeled temporal standard deviations for n=5 run years) without
307 treating BC as IN, which is a warming effect. The positive DRE from global solid fuel cookstove
308 emissions shows large spatial variability, with the largest impacts located over western Africa,
309 followed by India and China (figure not shown). The contributions of BC and POM to DRE are
310 $+105 \pm 4$ (warming) and -14 ± 1 (cooling) mW m⁻², respectively. In other words, the warming
311 effect of BC is partially offset by the cooling effect from POM. Additional cooling effects may
312 come from sulfate and SOA. CAM5-Chem assumes that BC is internally mixed with other
313 components in the accumulation mode and simulates enhanced absorption (BC mass absorption
314 cross section = 14.6 m² g⁻¹) when BC is coated by soluble aerosol components and water vapor
315 (Ghan et al., 2012), which results in larger estimates of the DRE than for BC alone (Bond et al.,
316 2013; Jacobson, 2001b).

317 The DRE from Indian solid fuel cookstove emissions also corresponds to a net warming effect
318 (Fig. 6), with a global annual mean value of $+11 \pm 1$ mW m⁻². Large impacts are found over
319 continental India, the Tibetan Plateau and southeastern China. On a global annual basis, DRE

320 values from BC and POM emissions from the Indian solid fuel cookstove sector are $+18 \pm 1$ and -
321 $3 \pm 0.2 \text{ mW m}^{-2}$, respectively.

322 **3.4.2 Aerosol indirect, semi-direct and surface albedo effects: BC not active as IN**

323 Global annual mean AIE and SAE values from global and Indian solid fuel cookstove aerosol
324 emissions are shown in Figure 6. In our study, AIE includes the first (albedo) and second (lifetime)
325 indirect effects, as well as the semi-direct effect. Annually averaged AIE from the global solid fuel
326 cookstove sector is $-226 \pm 5 \text{ mW m}^{-2}$ (Fig. 6), with annual mean shortwave (SW) AIE -122 ± 22
327 mW m^{-2} and longwave (LW) AIE $-104 \pm 17 \text{ mW m}^{-2}$, without treating BC as IN. Both the annual
328 mean SW and LW AIE thus yield cooling effects. The cooling signals of SW AIE mainly occur
329 over the western coast of South America, west and east coasts of Africa, South China and Himalaya
330 regions (figure not shown). This is directly linked to the contribution of global solid fuel cookstove
331 aerosol emissions to CCN (Pierce et al., 2007), which increases the cloud droplet number
332 concentrations (CDNC) and cloud liquid water path (CLWP). Figure 7 shows the global vertically-
333 integrated distribution of CLWP from the contribution of global solid fuel cookstove aerosol
334 emissions. The higher CLWP is due to the enhanced lifetime of liquid and mixed-phase clouds,
335 which therefore reflect more solar radiation, leading to cooling effect. For the LW AIE, the largest
336 cooling effect is found over tropical regions, especially over southern India and the Indian Ocean.
337 In order to investigate the causes of the LW AIE cooling effect, we analyze the cloud fraction
338 change over a defined region (Latitude:0-20°N; Longitude:60-90°E) due to the effect from the
339 global solid fuel cookstove sector. As shown in Figure 8a, cloud fraction in the lower troposphere
340 increases. However, in the middle and upper troposphere cloud fraction decreases by up to 0.6%,
341 with the strongest decrease found at ~150 hPa. We further analyze the changes in shallow and deep
342 convective mass fluxes of moisture over the same domain. As shown in Figure 8b, moist shallow
343 convective mass flux generally shows increases in the lower troposphere, which means that solid
344 fuel cookstove aerosol emissions enhance the convective transport of water vapor within the
345 boundary layer. By contrast, the deep convective mass flux demonstrates decreases from surface
346 up to the middle troposphere (Fig. 8c). This indicates that solid fuel cookstove aerosol emissions
347 may stabilize the boundary layer and inhibit the transport of water vapor from the surface to the
348 upper troposphere/lower stratosphere, which leads to decreases in ice cloud formation, thus

349 reducing cloud cover in the upper troposphere and lower stratosphere (UTLS) region at around
350 200 hPa (Fig. 8a) and a LW AIE cooling effect.

351 The global annual mean AIE from Indian solid fuel cookstove aerosol emissions accounts for
352 approximately 10% ($-22 \pm 3 \text{ mW m}^{-2}$) relative to the value of AIE from the global solid fuel
353 cookstove sector (Fig. 6), with globally averaged SW and LW AIE values of -3 ± 11 and -19 ± 11
354 mW m^{-2} respectively.

355 Global annual mean SAE values from global and Indian solid fuel cookstove sector are relatively
356 small: $+15 \pm 3$ and $-2 \pm 3 \text{ mW m}^{-2}$, respectively (Fig. 6). The warming effect is mainly due to the
357 deposition of BC on the surface of snow and sea ice (Flanner et al., 2007; Ghan, 2013; Ghan et al.,
358 2012).

359 **3.4.3 Total radiative effect: BC not active as IN**

360 The net total radiative effect of global and Indian solid fuel cookstove aerosol emissions are both
361 cooling, with the global annual mean estimated to be -141 ± 4 and $-12 \pm 4 \text{ mW m}^{-2}$ respectively
362 (Fig. 6). This suggests that if we remove solid fuel cookstove aerosol emissions, it will result in
363 warming and thus slightly increased global surface air temperature. That being said, this is likely
364 to be quite sensitive to model representation of aerosol mixing state (Fierce et al., 2017).

365 **3.4.4 Total radiative effect: BC active as IN**

366 For the radiative effect of global solid fuel cookstove emissions with BC as IN, global annual mean
367 DRE is $105 \pm 13 \text{ mW m}^{-2}$ (\pm represents standard deviations from modeling results with BC MFE
368 values as 0.01, 0.05 and 0.1), ranging from $+90$ to $+115 \text{ mW m}^{-2}$, which is 29-64% higher than the
369 DRE values from the default scheme (Fig. 6). Intriguingly, large globally averaged negative SW
370 AIE ($-1.36 \pm 0.63 \text{ W m}^{-2}$) and positive LW AIE ($+1.18 \pm 0.44 \text{ W m}^{-2}$) for global solid fuel
371 cookstove aerosol emissions are found, with annual mean values for the SW AIE ranging from -
372 1.83 to -0.64 W m^{-2} and from $+0.67$ to $+1.45 \text{ W m}^{-2}$ for the LW AIE. This results in a rather
373 uncertain net AIE, with a global annual mean AIE of $-177 \pm 223 \text{ mW m}^{-2}$ (Fig. 6). The reason for
374 the large global annual average negative SW AIE and positive LW AIE is a substantial increase in
375 high cloud ($< 500 \text{ hPa}$) fractions when BC acts as an efficient IN. For instance, with MFE = 0.1,
376 large increases (by up to 9%) in high cloud fractions from global solid fuel cookstove aerosol

377 emissions are found over subtropical regions, especially over the southern Atlantic Ocean (Fig. 9).
378 With BC particles active as IN, ice particle sizes become smaller, leading to a slower settling
379 velocity for ice particles and thus an increase in the lifetime of ice clouds. Increases in high clouds
380 not only reflect more solar radiation back to space, but also trap more LW radiation within the
381 troposphere. For SAE, the global annual mean value is $+12 \pm 10 \text{ mW m}^{-2}$ (Fig. 6). As a result, the
382 net total radiative effect of global solid fuel cookstove aerosol emissions ranges from -275 to +
383 154 mW m^{-2} , with a global annual mean of $-59 \pm 215 \text{ mW m}^{-2}$ (Fig. 6). Again, the source of the
384 large uncertainty of the total radiative effect is due to the choice of MFE values. With $\text{MFE} = 0.01$,
385 the global mean LW AIE ($+672 \text{ mW m}^{-2}$) outweighs SW AIE (-638 mW m^{-2}), and therefore results
386 in a net warming effect. For other MFE values (0.05 and 0.1), the absolute global annual mean SW
387 AIE values are always higher than the LW AIE, leading to a net negative (i.e., cooling) total
388 radiative effect.

389 For the Indian solid fuel cookstove sector, the global annual mean net total radiative effect is 0.3
390 $\pm 29 \text{ mW m}^{-2}$, with an AIE of -18 ± 37 and a SAE of $+1 \pm 8 \text{ mW m}^{-2}$, respectively.

391 **4 Discussion and Summary**

392 In this study, we employ the atmospheric component of a global 3-D climate model CESM v1.2.2,
393 CAM5.3-Chem, to investigate the impacts of solid fuel cookstove emissions on global climate
394 change. We update the default anthropogenic emission inventory using IIASA ECLIPSE V5a for
395 the year 2010. We focus our analysis on the radiative effects of global and Indian solid fuel
396 cookstove aerosol emissions. Model performance is evaluated against a global dataset of BC and
397 OA measurements from surface sites and AOD from AERONET. Compared with observations,
398 the model successfully reproduces the spatial patterns of atmospheric BC and OA concentrations,
399 and generally agrees with measurements to within a factor of 2. Globally, the simulated AOD
400 agrees quite well with observations, with NMB values close to zero. Nevertheless, the model tends
401 to underestimate AOD values over source regions (except for Africa) and overestimate AOD over
402 remote regions. The underestimates of AOD over India and China indicate that anthropogenic
403 emissions of carbonaceous aerosols and sulfate precursors in ECLIPSE V5a are underestimated
404 because carbonaceous aerosols and sulfate account for over 60% of the AOD over these two
405 countries (Lu et al., 2011; Streets et al., 2009), which may introduce uncertainties for our climate

406 estimates. The simulations reflect a present-day climatology forced with recycled year 2010
407 anthropogenic emissions. Model simulated BC concentrations were sampled in exact
408 correspondence to the observed temporal period. In some limited cases, OA and AOD are not
409 exactly temporally consistent with the available aerosol measurement network climatologies
410 applied in the evaluation. For regions where carbonaceous aerosol emissions have undergone
411 substantial changes over short periods in the past few years, the model-measurement comparison
412 may therefore introduce additional uncertainty. However, we focus the evaluation on the large-
413 scale regional aerosol system dynamics. In the control simulation, the global annual mean BC
414 burden and lifetime are 0.12 ± 0.001 Tg and 4.5 ± 0.04 days. For POM, the burden and lifetime
415 are 0.66 ± 0.006 Tg and 4.8 ± 0.04 days. Annual mean surface BC (POM) concentrations over
416 Northern India, East China and sub-Saharan Africa are 1.55 ± 0.076 , 0.76 ± 0.028 and 0.11 ± 0.004
417 $\mu\text{g m}^{-3}$ (7.11 ± 0.32 , 3.95 ± 0.12 and 0.48 ± 0.02 $\mu\text{g m}^{-3}$), respectively. BC and POM burdens from
418 global solid fuel cookstove emissions are 0.029 ± 0.001 and 0.13 ± 0.004 Tg, while contributions
419 from the Indian sector are 0.006 ± 0.000 and 0.027 ± 0.004 Tg, respectively.

420 In the default CESM simulations without treating BC as IN, globally averaged DRE values from
421 global and Indian solid fuel cookstove emissions are $+70 \pm 3$ and $+11 \pm 1$ mW m^{-2} , respectively.
422 The contributions of BC and POM from global solid fuel cookstove emissions to the DRE are
423 $+105 \pm 4$ and -14 ± 1 mW m^{-2} . Global annual mean SW and LW AIE values from global solid fuel
424 cookstove emissions are -122 ± 22 and -104 ± 17 mW m^{-2} , with contributions from India yielding
425 -3 ± 11 mW m^{-2} for the SW AIE and -19 ± 11 mW m^{-2} for the LW AIE, respectively. The cooling
426 effect of the SW AIE is associated with the increases of CCN and CDNC, whereas the negative
427 effects of LW AIE are caused by the suppression of convection that transports water vapor from
428 lower troposphere to upper troposphere/stratosphere, thus reducing ice cloud cover. The CAM5-
429 Chem also computes the SAE, with global and Indian solid fuel cookstove emissions contributing
430 $+15 \pm 3$ and -2 ± 3 mW m^{-2} , respectively. As a result, the net total radiative effects of global and
431 Indian solid fuel cookstove emissions are -141 ± 4 and -12 ± 4 mW m^{-2} , respectively, both
432 producing a net cooling effect.

433 Sensitivity studies are carried out to examine the impacts of global and Indian solid fuel cookstove
434 emissions on climate by treating BC as an effective IN, with MFE as 0.01, 0.05 and 0.1,
435 respectively. For the radiative impacts of global solid fuel cookstove emissions, global annual

436 mean DRE is $+105 \pm 13 \text{ mW m}^{-2}$, which is $\sim 50\%$ higher than the default model scheme in which
437 BC particles are not treated as IN (Fig. 6). This is driven by the increases of BC burden (due to
438 prolonged BC lifetimes) from global solid fuel cookstove emissions by up to 17% with BC as IN.
439 Because the BC absorption effect dominates the DRE, increases in BC burden enhance the
440 magnitude of annual mean DRE (Jacobson, 2001a). Compared with the default model scheme,
441 significant changes in globally averaged SW AIE are found, with a global annual mean of $-1.36 \pm$
442 0.63 W m^{-2} , which is about an order of magnitude higher than that from the default scheme.
443 Moreover, in contrast to the cooling effect found in the default scheme, annual mean positive LW
444 AIE is simulated here ($+1.18 \pm 0.44 \text{ W m}^{-2}$). The above changes in cookstove emission induced
445 SW and LW AIE are caused by the substantial increases in high cloud ($< 500 \text{ hPa}$) fractions with
446 BC particles acting as IN by up to 9% due to the effect of solid fuel cookstove emissions. Large
447 increases in high cloud fractions are found mainly over tropical regions, especially over southern
448 Africa. For the SAE, similar to the model default scheme, the global annual mean value is $+12 \pm$
449 10 mW m^{-2} . Summing up the DRE, the AIE and the SAE, the net total radiative effect of global
450 solid fuel cookstove emissions is $-59 \pm 215 \text{ mW m}^{-2}$. For the Indian sector, the global mean total
451 radiative effect is $0.3 \pm 29 \text{ mW m}^{-2}$, with a net AIE -18 ± 37 and a SAE $+1 \pm 8 \text{ mW m}^{-2}$,
452 respectively.

453 We compare our simulation results with previous studies as shown in Figure 10. The globally
454 averaged DRE in our control simulation is more than four times higher than that from the baseline
455 simulation of Kodros et al. (2015), which assumes homogeneous particle mixing state (Fig. 10).
456 Annual emissions of BC from global solid fuel cookstove sector in our study (2.3 Tg C yr^{-1}) is
457 approximately 44% higher than that from global biofuel emissions (1.6 Tg C yr^{-1}) in Kodros et al.
458 (2015), which, to some extent, leads to differences in annual mean DRE values together with
459 different optical calculations. The annual mean DRE value from another study by Butt et al. (2016)
460 differs from ours in magnitude and sign, and concluded that annually averaged DRE from
461 residential combustion sources was -5 mW m^{-2} (Fig. 10). The negative effect of DRE in Butt et al.
462 (2016) is partially driven by the inclusion of SO_2 emissions ($8.9 \text{ Tg SO}_2 \text{ yr}^{-1}$) from commercial
463 coal combustion in the residential sector, leading to the cooling effect of sulfate and organic
464 aerosols outweighing the warming from BC. For AIE, our control simulation is 38 times higher
465 than that from Kodros et al. (2015) and over an order of magnitude higher than that from Butt et
466 al. (2016). Consistent with our study, Ward et al. (2012) also found a large AIE (-1.74 to 1.00 W

467 m⁻²) for carbonaceous aerosols from fires using CESM CAM4-Chem. Both Kodros et al. (2015)
468 and Butt et al. (2016) used offline radiative models to calculate AIE and only considered the first
469 (albedo) aerosol indirect effect, which may partially explain the AIE differences. As mentioned
470 earlier, the AIE in our study includes aerosol first and second indirect effects as well as the semi-
471 direct effect. Lacey and Henze (2015) estimated that the global surface air temperature changes
472 due to solid wood fuel removal ranged from -0.28 K (cooling) to +0.16 K (warming), with a central
473 estimate of -0.06 K (cooling). This cooling estimate is opposite to our study. However, we
474 acknowledge that there are fundamental differences in calculating the radiative effect between our
475 study and Lacey and Henze (2015), which employed absolute regional temperature potentials to
476 quantify the climate responses.

477 Cookstove intervention programs have been implemented in developing countries, such as China,
478 India and some African countries, to improve air quality and human health and to mitigate climate
479 change (Anenberg et al., 2017; Aung et al., 2016; Carter et al., 2016). Our results suggest that
480 large-scale efforts to replace inefficient cookstoves in developing countries with advanced
481 technologies is not likely to reduce global warming through aerosol reductions, and may even lead
482 to increased global warming when aerosol-cloud interactions are taken into account. Therefore,
483 without improved constraints on BC interactions with clouds, especially mixed-phase and ice
484 clouds, the net sign of the impacts of carbonaceous aerosols from solid fuel cookstoves on global
485 climate (warming or cooling) remains ambiguous. This study does not include the greenhouse gas
486 emission effects from the solid fuel cookstove sector, which may indeed be large enough to imply
487 a net warming global climate impact depending on time scale (Lacey et al., 2017).

488 **Acknowledgements**

489 This article was developed under Assistance Agreement No. R835421 awarded by the U.S.
490 Environmental Protection Agency to SEI. It has not been formally reviewed by EPA. The views
491 expressed in this document are solely those of the authors and do not necessarily reflect those of
492 the Agency. EPA does not endorse any products or commercial services mentioned in this
493 publication. N. Unger acknowledges support from the University of Exeter, UK. The authors are
494 grateful to R. Bailis, A. Grieshop, J. Marshall, and H. Zerriffi for helpful discussions and
495 conversations that guided the manuscript development. We are thankful for helpful discussions

496 with S. Tilmes and S. Ghan. This project was supported in part by the facilities and staff of the
497 Yale University High Performance Computing Center.

498 **References**

499 Amann, M., Bertok, I., Borcken-Kleefeld, J., Cofala, J., Heyes, C., Höglund-Isaksson, L.,
500 Klimont, Z., Nguyen, B., Posch, M., Rafaj, P., Sandler, R., Schöpp, W., Wagner, F. and
501 Winiwarter, W.: Cost-effective control of air quality and greenhouse gases in Europe: Modeling
502 and policy applications, *Environ. Model. Softw.*, 26(12), 1489–1501,
503 doi:10.1016/j.envsoft.2011.07.012, 2011.

504 Amann, M., Klimont, Z. and Wagner, F.: Regional and Global Emissions of Air Pollutants:
505 Recent Trends and Future Scenarios, *Annu. Rev. Environ. Resour.*, 38(1), 31–55,
506 doi:10.1146/annurev-environ-052912-173303, 2013.

507 Anenberg, S. C., Henze, D. K., Lacey, F., Irfan, A., Kinney, P., Kleiman, G. and Pillarisetti, A.:
508 Air pollution-related health and climate benefits of clean cookstove programs in Mozambique,
509 *Environ. Res. Lett.*, 12(2), 25006, doi:10.1088/1748-9326/aa5557, 2017.

510 Archer-Nicholls, S., Carter, E., Kumar, R., Xiao, Q., Liu, Y., Frostad, J., Forouzanfar, M. H.,
511 Cohen, A., Brauer, M., Baumgartner, J. and Wiedinmyer, C.: The regional impacts of cooking
512 and heating emissions on ambient air quality and disease burden in China, *Environ. Sci.*
513 *Technol.*, 50(17), 9416–9423, doi:10.1021/acs.est.6b02533, 2016.

514 Aung, T. W., Jain, G., Sethuraman, K., Baumgartner, J., Reynolds, C., Grieshop, A. P., Marshall,
515 J. D. and Brauer, M.: Health and Climate-Relevant Pollutant Concentrations from a Carbon-
516 Finance Approved Cookstove Intervention in Rural India, *Environ. Sci. Technol.*, 50(13), 7228–
517 7238, doi:10.1021/acs.est.5b06208, 2016.

518 Barahona, D. and Nenes, A.: Parameterization of cirrus cloud formation in large-scale models:
519 Homogeneous nucleation, *J. Geophys. Res. Atmos.*, 113(11), 1–15, doi:10.1029/2007JD009355,
520 2008.

521 Barahona, D. and Nenes, A.: Parameterizing the competition between homogeneous and
522 heterogeneous freezing in ice cloud formation – polydisperse ice nuclei, *Atmos. Chem. Phys.*, 9,

523 5933–5948, doi:10.5194/acp-9-5933-2009, 2009.

524 Bauer, S. E., Menon, S., Koch, D., Bond, T. C. and Tsigaridis, K.: A global modeling study on
525 carbonaceous aerosol microphysical characteristics and radiative effects, *Atmos. Chem. Phys.*,
526 10(15), 7439–7456, doi:10.5194/acp-10-7439-2010, 2010.

527 Bond, T., Venkataraman, C. and Masera, O.: Global atmospheric impacts of residential fuels,
528 *Energy Sustain. Dev.*, 8(3), 20–32, doi:10.1016/S0973-0826(08)60464-0, 2004.

529 Bond, T. C., Doherty, S. J., Fahey, D. W., Forster, P. M., Berntsen, T., Deangelo, B. J., Flanner,
530 M. G., Ghan, S., Kärcher, B., Koch, D., Kinne, S., Kondo, Y., Quinn, P. K., Sarofim, M. C.,
531 Schultz, M. G., Schulz, M., Venkataraman, C., Zhang, H., Zhang, S., Bellouin, N., Guttikunda,
532 S. K., Hopke, P. K., Jacobson, M. Z., Kaiser, J. W., Klimont, Z., Lohmann, U., Schwarz, J. P.,
533 Shindell, D., Storelvmo, T., Warren, S. G. and Zender, C. S.: Bounding the role of black carbon
534 in the climate system: A scientific assessment, *J. Geophys. Res. Atmos.*, 118(11), 5380–5552,
535 doi:10.1002/jgrd.50171, 2013.

536 Bonjour, S., Wolf, J. and Lahiff, M.: Solid Fuel Use for Household Cooking: Country and
537 Regional Estimates for 1980–2010, *Environ. Health Perspect.*, 121(7), 784–790,
538 doi:10.1289/ehp.1205987, 2013.

539 Boucher, O., Randall, D., Artaxo, P., Bretherton, C., Feingold, G., Forster, P., Kerminen, V.-M.
540 V.-M., Kondo, Y., Liao, H., Lohmann, U., Rasch, P., Satheesh, S. K., Sherwood, S., Stevens, B.,
541 Zhang, X. Y. and Zhan, X. Y.: Clouds and Aerosols, *Clim. Chang. 2013 Phys. Sci. Basis.*
542 *Contrib. Work. Gr. I to Fifth Assess. Rep. Intergov. Panel Clim. Chang.*, 571–657,
543 doi:10.1017/CBO9781107415324.016, 2013.

544 Butt, E. W., Rap, A., Schmidt, A., Scott, C. E., Pringle, K. J., Reddington, C. L., Richards, N. A.
545 D., Woodhouse, M. T., Ramirez-Villegas, J., Yang, H., Vakkari, V., Stone, E. A., Rupakheti, M.,
546 Praveen, P. S., Van Zyl, P. G., Beukes, J. P., Josipovic, M., Mitchell, E. J. S., Sallu, S. M.,
547 Forster, P. M. and Spracklen, D. V.: The impact of residential combustion emissions on
548 atmospheric aerosol, human health, and climate, *Atmos. Chem. Phys.*, 16(2), 873–905,
549 doi:10.5194/acp-16-873-2016, 2016.

550 Carter, E., Archer-Nicholls, S., Ni, K., Lai, A. M., Niu, H., Secret, M. H., Sauer, S. M., Schauer,
551 J. J., Ezzati, M., Wiedinmyer, C., Yang, X. and Baumgartner, J.: Seasonal and Diurnal Air
552 Pollution from Residential Cooking and Space Heating in the Eastern Tibetan Plateau, *Environ.*
553 *Sci. Technol.*, 50(15), 8353–8361, doi:10.1021/acs.est.6b00082, 2016.

554 Chow, J. C., Watson, J. G., Pritchett, L. C., Pierson, W. R., Frazer, C. A. and Purcell, R. G.: THE
555 DRI THERMAL/OPTICAL REFLECTANCE CARBON ANALYSIS SYSTEM :
556 DESCRIPTION, EVALUATION A N D APPLICATIONS IN U.S. AIR QUALITY STUDIES,
557 *Atmos. Environ.*, 27A(8), 1185–1201, 1993.

558 Chow, J. C., Watson, J. G., Chen, L.-W. A., Arnott, W. P. and Moosmuller, H.: Equivalence of
559 Elemental Carbon by Thermal/Optical Reflectance and Transmittance with Different
560 Temperature Protocols, *Environ. Sci. Technol.*, 38(16), 4414–4422, 2004.

561 Chung, S. H.: Climate response of direct radiative forcing of anthropogenic black carbon, *J.*
562 *Geophys. Res.*, 110(D11), D11102, doi:10.1029/2004JD005441, 2005.

563 Chung, S. H. and Seinfeld, J. H.: Global distribution and climate forcing of carbonaceous
564 aerosols, *J. Geophys. Res. Atmos.*, 107(19), doi:10.1029/2001JD001397, 2002.

565 Chylek, P. and Wong, J.: Effect of absorbing aerosols on global radiation budget, *Geophys. Res.*
566 *Lett.*, 22(8), 929–931, 1995.

567 Cozic, J., Mertes, S., Verheggen, B., Cziczo, D. J., Gallavardin, S. J., Walter, S., Baltensperger,
568 U. and Weingartner, E.: Black carbon enrichment in atmospheric ice particle residuals observed
569 in lower tropospheric mixed phase clouds, *J. Geophys. Res. Atmos.*, 113(15), 1–11,
570 doi:10.1029/2007JD009266, 2008.

571 DeMott, P. J., Chen, Y., Kreidenweis, S. M., Rogers, D. C. and Sherman, D. E.: Ice formation by
572 black carbon particles, *Geophys. Res. Lett.*, 26(16), 2429–2432, doi:10.1029/1999GL900580,
573 1999.

574 Dubovikl, O. and King, M. D.: A flexible inversion algorithm for retrieval of aerosol optical
575 properties from Sun and sky radiance measurements, *J. Geophys. Res.*, 105696(27), 673–20,
576 doi:10.1029/2000JD900282, 2000.

577 EMEP/MSC-W, EMEP/CCC, EMEP/CEIP, IDAEA-CSIC, CCE/RIVM and FMI:
578 Transboundary particulate matter, photo-oxidants, acidifying and eutrophying components.,
579 2014.

580 Emmons, L. K., Walters, S., Hess, P. G., Lamarque, J.-F., Pfister, G. G., Fillmore, D., Granier,
581 C., Guenther, A., Kinnison, D., Laepple, T., Orlando, J., Tie, X., Tyndall, G., Wiedinmyer, C.,
582 Baughcum, S. L. and Kloster, S.: Description and evaluation of the Model for Ozone and Related
583 chemical Tracers, version 4 (MOZART-4), *Geosci. Model Dev.*, 3, 43–67, doi:10.5194/gmd-3-
584 43-2010, 2010.

585 Ezzati, M. and Kammen, D. M.: The health impacts of exposure to indoor air pollution from
586 solid fuels in developing countries: Knowledge, gaps, and data needs, *Environ. Health Perspect.*,
587 110(11), 1057–1068, doi:10.1289/ehp.021101057, 2002.

588 Fierce, L., Riemer, N. and Bond, T. C.: Toward reduced representation of mixing state for
589 simulating aerosol effects on climate, *Bull. Am. Meteorol. Soc.*, 98(5), 971–980,
590 doi:10.1175/BAMS-D-16-0028.1, 2017.

591 Flanner, M. G., Zender, C. S., Randerson, J. T. and Rasch, P. J.: Present-day climate forcing and
592 response from black carbon in snow, *J. Geophys. Res. Atmos.*, 112(11), 1–17,
593 doi:10.1029/2006JD008003, 2007.

594 Gadhavi, H. S., Renuka, K., Ravi Kiran, V., Jayaraman, A., Stohl, A., Klimont, Z. and Beig, G.:
595 Evaluation of black carbon emission inventories using a Lagrangian dispersion model - A case
596 study over southern India, *Atmos. Chem. Phys.*, 15(3), 1447–1461, doi:10.5194/acp-15-1447-
597 2015, 2015.

598 Garland, C., Delapena, S., Prasad, R., L'Orange, C., Alexander, D. and Johnson, M.: Black
599 carbon cookstove emissions: A field assessment of 19 stove/fuel combinations, *Atmos. Environ.*,
600 169, 140–149, doi:10.1016/j.atmosenv.2017.08.040, 2017.

601 GBD 2015 Risk Factors Collaborators: Global, regional, and national comparative risk
602 assessment of 79 behavioural, environmental and occupational, and metabolic risks or clusters of
603 risks, 1990–2015: a systematic analysis for the Global Burden of Disease Study 2015, *Lancet*,

604 388(10053), 1659–1724, doi:10.1016/S0140-6736(16)31679-8, 2016.

605 Gettelman, A., Liu, X., Barahona, D., Lohmann, U. and Chen, C.: Climate impacts of ice
606 nucleation, *J. Geophys. Res. Atmos.*, 117(20), 1–14, doi:10.1029/2012JD017950, 2012.

607 Ghan, S. J.: Technical note: Estimating aerosol effects on cloud radiative forcing, *Atmos. Chem.*
608 *Phys.*, 13(19), 9971–9974, doi:10.5194/acp-13-9971-2013, 2013.

609 Ghan, S. J., Liu, X., Easter, R. C., Zaveri, R., Rasch, P. J., Yoon, J. H. and Eaton, B.: Toward a
610 minimal representation of aerosols in climate models: Comparative decomposition of aerosol
611 direct, semidirect, and indirect radiative forcing, *J. Clim.*, 25(19), 6461–6476, doi:10.1175/JCLI-
612 D-11-00650.1, 2012.

613 Hanbar, R. D. and Karve, P.: National Programme on Improved Chulha (NPIC) of the
614 Government of India: An overview, *Energy Sustain. Dev.*, 6(2), 49–55, doi:10.1016/S0973-
615 0826(08)60313-0, 2002.

616 He, C., Li, Q. B., Liou, K. N., Zhang, J., Qi, L., Mao, Y., Gao, M., Lu, Z., Streets, D. G., Zhang,
617 Q., Sarin, M. M. and Ram, K.: A global 3-D CTM evaluation of black carbon in the Tibetan
618 Plateau, *Atmos. Chem. Phys.*, 14(13), 7091–7112, doi:10.5194/acp-14-7091-2014, 2014.

619 He, J. and Zhang, Y.: Improvement and further development in CESM/CAM5: Gas-phase
620 chemistry and inorganic aerosol treatments, *Atmos. Chem. Phys.*, 14(17), 9171–9200,
621 doi:10.5194/acp-14-9171-2014, 2014.

622 Holben, B. N., Eck, T. F., Slutsker, I., Tanré, D., Buis, J. P., Setzer, A., Vermote, E., Reagan, J.
623 A., Kaufman, Y. J., Nakajima, T., Lavenu, F., Jankowiak, I. and Smirnov, A.: AERONET—A
624 Federated Instrument Network and Data Archive for Aerosol Characterization, *Remote Sens.*
625 *Environ.*, 66(1), 1–16, doi:10.1016/S0034-4257(98)00031-5, 1998.

626 Holben, B. N., Tanré, D., Smirnov, a., Eck, T. F., Slutsker, I., Abuhassan, N., Newcomb, W. W.,
627 Schafer, J. S., Chatenet, B., Lavenu, F., Kaufman, Y. J., Castle, J. Vande, Setzer, a., Markham,
628 B., Clark, D., Frouin, R., Halthore, R., Karneli, a., O’Neill, N. T., Pietras, C., Pinker, R. T.,
629 Voss, K. and Zibordi, G.: An emerging ground-based aerosol climatology: Aerosol optical depth
630 from AERONET, *J. Geophys. Res.*, 106(D11), 12067, doi:10.1029/2001JD900014, 2001.

631 Huang, Y., Wu, S., Dubey, M. K. and French, N. H. F.: Impact of aging mechanism on model
632 simulated carbonaceous aerosols, *Atmos. Chem. Phys.*, 13(13), 6329–6343, doi:10.5194/acp-13-
633 6329-2013, 2013.

634 Jacobson, M. Z.: Global direct radiative forcing due to multicomponent natural and anthropogenic
635 aerosols, *J. Geophys. Res.*, 106(D2), 1551–1568, doi:10.1029/2000JD900514, 2001a.

636 Jacobson, M. Z.: Strong radiative heating due to the mixing state of black carbon in atmospheric
637 aerosols., *Nature*, 409(6821), 695–697, doi:10.1038/35055518, 2001b.

638 Janssens-Maenhout, G., Crippa, M., Guizzardi, D., Dentener, F., Muntean, M., Pouliot, G.,
639 Keating, T., Zhang, Q., Kurokawa, J., Wankmüller, R., Denier van der Gon, H., Kuenen, J. J. P.,
640 Klimont, Z., Frost, G., Darras, S., Koffi, B. and Li, M.: HTAP_v2.2: a mosaic of regional and
641 global emission grid maps for 2008 and 2010 to study hemispheric transport of air pollution,
642 *Atmos. Chem. Phys.*, 15(19), 11411–11432, doi:10.5194/acp-15-11411-2015, 2015.

643 Kanagawa, M. and Nakata, T.: Analysis of the energy access improvement and its socio-
644 economic impacts in rural areas of developing countries, *Ecol. Econ.*, 62(2), 319–329,
645 doi:10.1016/j.ecolecon.2006.06.005, 2007.

646 Karcher, B. and Hendricks, J.: Physically based parameterization of cirrus cloud formation for
647 use in global atmospheric models, *J. Geophys. Res.*, 111, D01205, doi:10.1029/2005JD006219,
648 2006.

649 Kishore, V. V. N. and Ramana, P. V.: Improved cookstoves in rural India: How improved are
650 they? A critique of the perceived benefits from the National Programme on Improved Chulhas
651 (NPIC), *Energy*, 27(1), 47–63, doi:10.1016/S0360-5442(01)00056-1, 2002.

652 Klimont, Z., Cofala, J., Wei, W., Zhang, C., Wang, S., Kejun, J., Bhandari, P., Mathur, R.,
653 Purohit, P., Rafaj, P., Chambers, A., Amann, M. and Hao, J.: Projections of SO₂, NO_x and
654 carbonaceous aerosols emissions in Asia, *Tellus, Ser. B Chem. Phys. Meteorol.*, (61B), 602–617,
655 doi:10.1111/j.1600-0889.2009.00428.x, 2009.

656 Klimont, Z., Kupiainen, K., Heyes, C., Purohit, P., Cofala, J., Rafaj, P., Borken-Kleefeld, J. and
657 Schöpp, W.: Global anthropogenic emissions of particulate matter including black carbon,

658 Atmos. Chem. Phys., 17(14), 8681–8723, doi:10.5194/acp-17-8681-2017, 2017.

659 Kodros, J. K., Scott, C. E., Farina, S. C., Lee, Y. H., L'Orange, C., Volckens, J. and Pierce, J. R.:
660 Uncertainties in global aerosols and climate effects due to biofuel emissions, Atmos. Chem.
661 Phys., 15(15), 8577–8596, doi:10.5194/acp-15-8577-2015, 2015.

662 Koehler, K. A., DeMott, P. J., Kreidenweis, S. M., Popovicheva, O. B., Petters, M. D., Carrico,
663 C. M., Kireeva, E. D., Khokhlova, T. D. and Shonija, N. K.: Cloud condensation nuclei and ice
664 nucleation activity of hydrophobic and hydrophilic soot particles, Phys. Chem. Chem. Phys.,
665 11(36), 7906–7920, doi:10.1039/b916865f, 2009.

666 Kooperman, G. J., Pritchard, M. S., Ghan, S. J., Wang, M., Somerville, R. C. J. and Russell, L.
667 M.: Constraining the influence of natural variability to improve estimates of global aerosol
668 indirect effects in a nudged version of the Community Atmosphere Model 5, J. Geophys. Res.
669 Atmos., 117(23), 1–16, doi:10.1029/2012JD018588, 2012.

670 Kulkarni, G., China, S., Liu, S., Nandasiri, M., Sharma, N., Wilson, J., Aiken, A. C., Chand, D.,
671 Laskin, A., Mazzoleni, C., Pekour, M., Shilling, J., Shutthanandan, V., Zelenyuk, A. and Zaveri,
672 R. A.: Ice nucleation activity of diesel soot particles at cirrus relevant temperature conditions:
673 Effects of hydration, secondary organics coating, soot morphology, and coagulation, Geophys.
674 Res. Lett., 43(7), 3580–3588, doi:10.1002/2016GL068707, 2016.

675 Lacey, F. and Henze, D.: Global climate impacts of country-level primary carbonaceous aerosol
676 from solid-fuel cookstove emissions, Environ. Res. Lett., 10(11), 114003, doi:10.1088/1748-
677 9326/10/11/114003, 2015.

678 Lacey, F. G., Henze, D. K., Lee, C. J., van Donkelaar, A. and Martin, R. V.: Transient climate
679 and ambient health impacts due to national solid fuel cookstove emissions, Proc. Natl. Acad.
680 Sci., 114(6), 1269–1274, doi:10.1073/pnas.1612430114, 2017.

681 Lamarque, J. F., Emmons, L. K., Hess, P. G., Kinnison, D. E., Tilmes, S., Vitt, F., Heald, C. L.,
682 Holland, E. A., Lauritzen, P. H., Neu, J., Orlando, J. J., Rasch, P. J. and Tyndall, G. K.: CAM-
683 chem: Description and evaluation of interactive atmospheric chemistry in the Community Earth
684 System Model, Geosci. Model Dev., 5(2), 369–411, doi:10.5194/gmd-5-369-2012, 2012.

685 Legros, G., Havet, I., Bruce, N. and Bonjour, S.: The Energy Access Situation in Developing
686 Countries, WHO UNDP, 142 [online] Available from:
687 <http://scholar.google.com/scholar?hl=en&btnG=Search&q=intitle:THE+ENERGY+ACCESS+SITUATION+IN+DEVELOPING+COUNTRIES+A+Review+Focusing+on+the#0>, 2009.
688

689 Lelieveld, J., Evans, J. S., Fnais, M., Giannadaki, D. and Pozzer, A.: The contribution of outdoor
690 air pollution sources to premature mortality on a global scale, *Nature*, 525(7569), 367–371,
691 doi:10.1038/nature15371, 2015.

692 Liu, J., Mauzerall, D. L., Chen, Q., Zhang, Q., Song, Y., Peng, W., Klimont, Z., Qiu, X., Zhang,
693 S., Hu, M., Lin, W., Smith, K. R. and Zhu, T.: Air pollutant emissions from Chinese households:
694 A major and underappreciated ambient pollution source, *Proc. Natl. Acad. Sci.*, 113(28), 7756–
695 7761, doi:10.1073/pnas.1604537113, 2016.

696 Liu, X. and Penner, J. E.: Ice nucleation parameterization for global models, *Meteorol.*
697 *Zeitschrift*, 14(4), 499–514, doi:10.1127/0941-2948/2005/0059, 2005.

698 Liu, X., Penner, J. E., Ghan, S. J. and Wang, M.: Inclusion of ice microphysics in the NCAR
699 Community Atmospheric Model version 3 (CAM3), *J. Clim.*, 20(18), 4526–4547,
700 doi:10.1175/JCLI4264.1, 2007.

701 Liu, X., Easter, R. C., Ghan, S. J., Zaveri, R., Rasch, P., Shi, X., Lamarque, J. F., Gettelman, A.,
702 Morrison, H., Vitt, F., Conley, A., Park, S., Neale, R., Hannay, C., Ekman, A. M. L., Hess, P.,
703 Mahowald, N., Collins, W., Iacono, M. J., Bretherton, C. S., Flanner, M. G. and Mitchell, D.:
704 Toward a minimal representation of aerosols in climate models: Description and evaluation in
705 the Community Atmosphere Model CAM5, *Geosci. Model Dev.*, 5(3), 709–739,
706 doi:10.5194/gmd-5-709-2012, 2012.

707 Lohmann, U.: A glaciation indirect aerosol effect caused by soot aerosols, *Geophys. Res. Lett.*,
708 29(4), 1052, doi:10.1029/2001gl014357, 2002.

709 Lohmann, U., Feichter, J., Penner, J. and Leaitch, R.: Indirect effect of sulfate and carbonaceous
710 aerosols: A mechanistic treatment, *J. Geophys. Res. Atmos.*, 105(D10), 12193–12206,
711 doi:10.1029/1999JD901199, 2000.

712 Lu, Z., Zhang, Q. and Streets, D. G.: Sulfur dioxide and primary carbonaceous aerosol emissions
713 in China and India, 1996-2010, *Atmos. Chem. Phys.*, 11(18), 9839–9864, doi:10.5194/acp-11-
714 9839-2011, 2011.

715 Malm, W. C., Sisler, J. F., Huffman, D., Eldred, R. A. and Cahill, T. A.: Spatial and seasonal
716 trends in particle concentration and optical extinction in the United States, *J. Geophys. Res.*,
717 99(D1), 1347–1370, doi:10.1029/93JD02916, 1994.

718 Myhre, G., Samset, B. H., Schulz, M., Balkanski, Y., Bauer, S., Berntsen, T. K., Bian, H.,
719 Bellouin, N., Chin, M., Diehl, T., Easter, R. C., Feichter, J., Ghan, S. J., Hauglustaine, D.,
720 Iversen, T., Kinne, S., Kirkevåg, A., Lamarque, J. F., Lin, G., Liu, X., Lund, M. T., Luo, G., Ma,
721 X., Van Noije, T., Penner, J. E., Rasch, P. J., Ruiz, A., Seland, Skeie, R. B., Stier, P., Takemura,
722 T., Tsigaridis, K., Wang, P., Wang, Z., Xu, L., Yu, H., Yu, F., Yoon, J. H., Zhang, K., Zhang, H.
723 and Zhou, C.: Radiative forcing of the direct aerosol effect from AeroCom Phase II simulations,
724 *Atmos. Chem. Phys.*, 13(4), 1853–1877, doi:10.5194/acp-13-1853-2013, 2013.

725 Pan, X., Chin, M., Gautam, R., Bian, H., Kim, D., Colarco, P. R., Diehl, T. L., Takemura, T. and
726 Pozzoli, L.: A multi-model evaluation of aerosols over South Asia : common, , 5903–5928,
727 doi:10.5194/acp-15-5903-2015, 2015.

728 Penner, J. E., Dickinson, R. E. and O'Neill, C. A.: Effects of Aerosol from Biomass Burning on
729 the Global Radiation Budget, *Science*, 256(5062), 1432–1435,
730 doi:10.1126/science.256.5062.1432, 1992.

731 Penner, J. E., Chen, Y., Wang, M. and Liu, X.: Possible influence of anthropogenic aerosols on
732 cirrus clouds and anthropogenic forcing, *Atmos. Chem. Phys.*, 9(3), 879–896, doi:10.5194/acp-9-
733 879-2009, 2009.

734 Pierce, J. R., Chen, K. and Adams, P. J.: Contribution of carbonaceous aerosol to cloud
735 condensation nuclei: processes and uncertainties evaluated with a global aerosol microphysics
736 model, *Atmos. Chem. Phys.*, 7, 5447–5466, doi:10.5194/acp-7-5447-2007, 2007.

737 Quennehen, B., Raut, J. C., Law, K. S., Daskalakis, N., Ancellet, G., Clerbaux, C., Kim, S. W.,
738 Lund, M. T., Myhre, G., Olivie, D. J. L., Safieddine, S., Skeie, R. B., Thomas, J. L., Tsyro, S.,

739 Bazureau, A., Bellouin, N., Hu, M., Kanakidou, M., Klimont, Z., Kupiainen, K.,
740 Myriokefalitakis, S., Quaas, J., Rumbold, S. T., Schulz, M., Cherian, R., Shimizu, A., Wang, J.,
741 Yoon, S. C. and Zhu, T.: Multi-model evaluation of short-lived pollutant distributions over east
742 Asia during summer 2008, *Atmos. Chem. Phys.*, 16(17), 10765–10792, doi:10.5194/acp-16-
743 10765-2016, 2016.

744 Reddington, C. L., Spracklen, D. V., Artaxo, P., Ridley, D. A., Rizzo, L. V. and Arana, A.:
745 Analysis of particulate emissions from tropical biomass burning using a global aerosol model
746 and long-term surface observations, *Atmos. Chem. Phys.*, 16(17), 11083–11106,
747 doi:10.5194/acp-16-11083-2016, 2016.

748 Riahi, K., Rao, S., Krey, V., Cho, C., Chirkov, V., Fischer, G., Kindermann, G., Nakicenovic, N.
749 and Rafaj, P.: RCP 8.5-A scenario of comparatively high greenhouse gas emissions, *Clim.*
750 *Change*, 109(1), 33–57, doi:10.1007/s10584-011-0149-y, 2011.

751 Schulz, M., Textor, C., Kinne, S., Balkanski, Y., Bauer, S., Berntsen, T., Berglen, T., Boucher,
752 O., Dentener, F., Guibert, S., Isaksen, I. S. a., Iversen, T., Koch, D., Kirkevåg, A., Liu, X.,
753 Montanaro, V., Myhre, G., Penner, J. E., Pitari, G., Reddy, S., Seland, Ø., Stier, P. and
754 Takemura, T.: Radiative forcing by aerosols as derived from the AeroCom present-day and pre-
755 industrial simulations, *Atmos. Chem. Phys.*, 6, 5225–5246, doi:10.5194/acpd-6-5095-2006,
756 2006.

757 Smith, K. R., Bruce, N., Balakrishnan, K., Adair-Rohani, H., Balmes, J., Chafe, Z., Dherani, M.,
758 Hosgood, H. D., Mehta, S., Pope, D. and Rehfuess, E.: Millions Dead: How Do We Know and
759 What Does It Mean? Methods Used in the Comparative Risk Assessment of Household Air
760 Pollution, *Annu. Rev. Public Health*, 35(1), 185–206, doi:10.1146/annurev-publhealth-032013-
761 182356, 2014.

762 Spracklen, D. V., Jimenez, J. L., Carslaw, K. S., Worsnop, D. R., Evans, M. J., Mann, G. W.,
763 Zhang, Q., Canagaratna, M. R., Allan, J., Coe, H., McFiggans, G., Rap, A. and Forster, P.:
764 Aerosol mass spectrometer constraint on the global secondary organic aerosol budget, *Atmos.*
765 *Chem. Phys.*, 11(23), 12109–12136, doi:10.5194/acp-11-12109-2011, 2011a.

766 Spracklen, D. V., Carslaw, K. S., Pöschl, U., Rap, A. and Forster, P. M.: Global cloud

767 condensation nuclei influenced by carbonaceous combustion aerosol, *Atmos. Chem. Phys.*,
768 11(17), 9067–9087, doi:10.5194/acp-11-9067-2011, 2011b.

769 Stohl, A., Aamaas, B., Amann, M., Baker, L. H., Bellouin, N., Berntsen, T. K., Boucher, O.,
770 Cherian, R., Collins, W., Daskalakis, N., Dusinska, M., Eckhardt, S., Fuglestedt, J. S., Harju,
771 M., Heyes, C., Hodnebrog, Hao, J., Im, U., Kanakidou, M., Klimont, Z., Kupiainen, K., Law, K.
772 S., Lund, M. T., Maas, R., MacIntosh, C. R., Myhre, G., Myriokefalitakis, S., Olivié, D., Quaas,
773 J., Quennehen, B., Raut, J. C., Rumbold, S. T., Samset, B. H., Schulz, M., Seland, Shine, K. P.,
774 Skeie, R. B., Wang, S., Yttri, K. E. and Zhu, T.: Evaluating the climate and air quality impacts of
775 short-lived pollutants, *Atmos. Chem. Phys.*, 15(18), 10529–10566, doi:10.5194/acp-15-10529-
776 2015, 2015.

777 Streets, D. G., Yan, F., Chin, M., Diehl, T., Mahowald, N., Schultz, M., Wild, M., Wu, Y. and
778 Yu, C.: Anthropogenic and natural contributions to regional trends in aerosol optical depth,
779 1980-2006, *J. Geophys. Res. Atmos.*, 114(14), 1–16, doi:10.1029/2008JD011624, 2009.

780 Textor, C., Schulz, M., Guibert, S., Kinne, S., Balkanski, Y., Bauer, S., Berntsen, T., Berglen, T.,
781 Boucher, O., Chin, M., Dentener, F., Diehl, T., Easter, R., Feichter, H., Fillmore, D., Ghan, S.,
782 Ginoux, P., Gong, S., Grini, A., Hendricks, J., Horowitz, L., Huang, P., Isaksen, I., Iversen, I.,
783 Kloster, S., Koch, D., Kirkevåg, A., Kristjansson, J. E., Krol, M., Lauer, A., Lamarque, J. F., Liu,
784 X., Montanaro, V., Myhre, G., Penner, J., Pitari, G., Reddy, S., Seland, Ø., Stier, P., Takemura,
785 T. and Tie, X.: Analysis and quantification of the diversities of aerosol life cycles within
786 AeroCom, *Atmos. Chem. Phys.*, 6(7), 1777–1813, doi:10.5194/acp-6-1777-2006, 2006.

787 Tilmes, S., Lamarque, J. F., Emmons, L. K., Kinnison, D. E., Ma, P. L., Liu, X., Ghan, S.,
788 Bardeen, C., Arnold, S., Deeter, M., Vitt, F., Ryerson, T., Elkins, J. W., Moore, F., Spackman, J.
789 R. and Val Martin, M.: Description and evaluation of tropospheric chemistry and aerosols in the
790 Community Earth System Model (CESM1.2), *Geosci. Model Dev.*, 8(5), 1395–1426,
791 doi:10.5194/gmd-8-1395-2015, 2015.

792 Venkataraman, C., Habib, G., Eiguren-Fernandez, A., Miguel, A. H. and Friendlander, S. K.:
793 Residential Biofuels in South Asia: Carbonaceous Aerosol Emissions and Climate Impacts,
794 *Science*, 307(5714), 1454–1456, doi:10.1126/science.1104359, 2005.

795 Venkataraman, C., Sagar, A. D., Habib, G., Lam, N. and Smith, K. R.: The Indian National
796 Initiative for Advanced Biomass Cookstoves: The benefits of clean combustion, *Energy Sustain.*
797 *Dev.*, 14(2), 63–72, doi:10.1016/j.esd.2010.04.005, 2010.

798 Wang, Q., Jacob, D. J., Fisher, J. A., Mao, J., Leibensperger, E. M., Carouge, C. C., Le Sager, P.,
799 Kondo, Y., Jimenez, J. L., Cubison, M. J. and Doherty, S. J.: Sources of carbonaceous aerosols
800 and deposited black carbon in the Arctic in winter-spring: Implications for radiative forcing,
801 *Atmos. Chem. Phys.*, 11(23), 12453–12473, doi:10.5194/acp-11-12453-2011, 2011.

802 Wang, Q., Jacob, D. J., Spackman, J. R., Perring, A. E., Schwarz, J. P., Moteki, N., Marais, E.
803 A., Ge, C., Wang, J. and Barrett, S. R. H.: Global budget and radiative forcing of black carbon
804 aerosol: Constraints from pole-to-pole (HIPPO) observations across the Pacific, *J. Geophys.*
805 *Res.*, 119(1), 195–206, doi:10.1002/2013JD020824, 2014a.

806 Wang, X., Heald, C. L., Ridley, D. A., Schwarz, J. P., Spackman, J. R., Perring, A. E., Coe, H.,
807 Liu, D. and Clarke, A. D.: Exploiting simultaneous observational constraints on mass and
808 absorption to estimate the global direct radiative forcing of black carbon and brown carbon,
809 *Atmos. Chem. Phys.*, 14(20), 10989–11010, doi:10.5194/acp-14-10989-2014, 2014b.

810 Ward, D. S., Kloster, S., Mahowald, N. M., Rogers, B. M., Randerson, J. T. and Hess, P. G.: The
811 changing radiative forcing of fires: global model estimates for past, present and future, *Atmos.*
812 *Chem. Phys.*, 12, 10857–10886, doi:10.5194/acp-12-10857-2012, 2012.

813 Zhang, L., Henze, D. K., Grell, G. A., Carmichael, G. R., Bousserez, N., Zhang, Q., Torres, O.,
814 Ahn, C., Lu, Z., Cao, J. and Mao, Y.: Constraining black carbon aerosol over Asia using OMI
815 aerosol absorption optical depth and the adjoint of GEOS-Chem, *Atmos. Chem. Phys.*, 15(18),
816 10281–10308, doi:10.5194/acp-15-10281-2015, 2015.

817 Zhang, Q., Jimenez, J. L., Canagaratna, M. R., Allan, J. D., Coe, H., Ulbrich, I., Alfarra, M. R.,
818 Takami, A., Middlebrook, A. M., Sun, Y. L., Dzepina, K., Dunlea, E., Docherty, K., DeCarlo, P.
819 F., Salcedo, D., Onasch, T., Jayne, J. T., Miyoshi, T., Shimo, A., Hatakeyama, S., Takegawa,
820 N., Kondo, Y., Schneider, J., Drewnick, F., Borrmann, S., Weimer, S., Demerjian, K., Williams,
821 P., Bower, K., Bahreini, R., Cottrell, L., Griffin, R. J., Rautiainen, J., Sun, J. Y., Zhang, Y. M.
822 and Worsnop, D. R.: Ubiquity and dominance of oxygenated species in organic aerosols in

823 anthropogenically-influenced Northern Hemisphere midlatitudes, *Geophys. Res. Lett.*, 34(13), 1–
824 6, doi:10.1029/2007GL029979, 2007.

825 Zheng, Y., Unger, N., Hodzic, A., Emmons, L., Knote, C., Tilmes, S., Lamarque, J. F. and Yu,
826 P.: Limited effect of anthropogenic nitrogen oxides on Secondary Organic Aerosol formation,
827 *Atmos. Chem. Phys.*, 15(23), 23231–23277, doi:10.5194/acpd-15-23231-2015, 2015.

828

829

830

831

832

833

834

835

836

837

838

839

840

841

842

843

844 **Table 1. Annual budget for various species for the BASE, GBLSF_OFF and INDSF_OFF**
 845 **simulations for the year 2010.**

Specie	ECLIPSE V5a (BASE) ^a	GBLSF_OFF ^a	INDSF_OFF ^a
BC	7.23	4.92	6.87
POM	18.9	8.53	17.2
SO ₂	98.5	97.1	98.37
NO _x	120.5	118	119.8
VOC	81.1	52.4	76.6
CO	548	358	516
NH ₃	54.9	54.6	54.87

846 ^aUnits are Tg specie/yr.

847

848

849

850

851

852

853

854

855

856

857 **Table 2. Model experiments setup.**

Experiments	Anthropogenic emission scenario
BASE	ECLIPSE V5a
GBLSF_OFF	ECLIPSE V5a excluding global solid fuel cookstove emissions
INDSF_OFF	ECLIPSE V5a excluding Indian solid fuel cookstove emissions

858

859

860

861

862

863

864

865

866

867

868

869

870

871

872 **Table 3. Global budgets, burden and lifetime of BC and POM from model control**
 873 **simulations.**

Specie	BC	POM
Sources (Tg specie/yr)	9.73	49.9
fossil fuel and biofuel	7.23	18.9
biomass burning emissions	2.5	31
Sinks (Tg specie/yr)	9.72	49.8
Dry Deposition	1.8	8.14
Wet Deposition	7.92	41.7
Burden (Tg) ^a	0.12 ± 0.001	0.66 ± 0.006
Lifetime (days) ^a	4.5 ± 0.04	4.8 ± 0.04

874 ^astandard deviation represents the uncertainty error owing to temporal variability in the
 875 model.

876

877

878

879

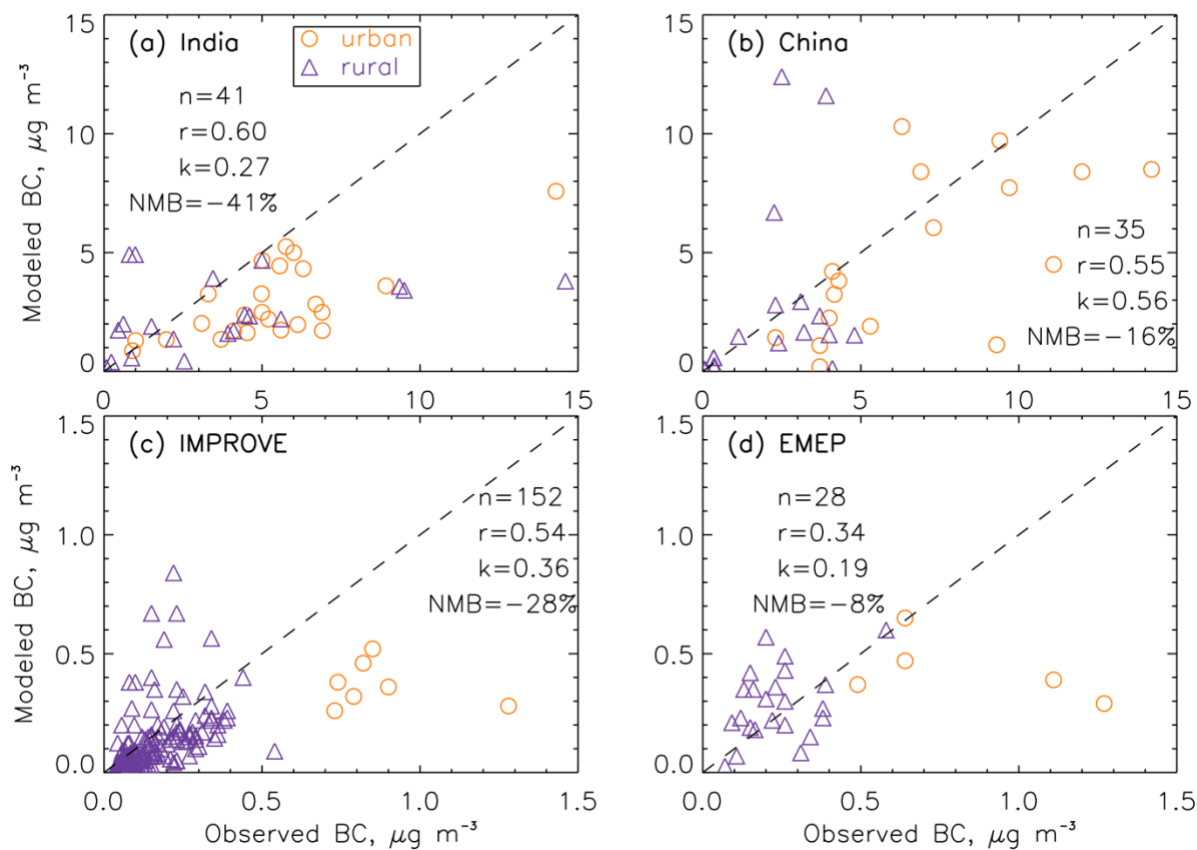
880

881

882

883

884



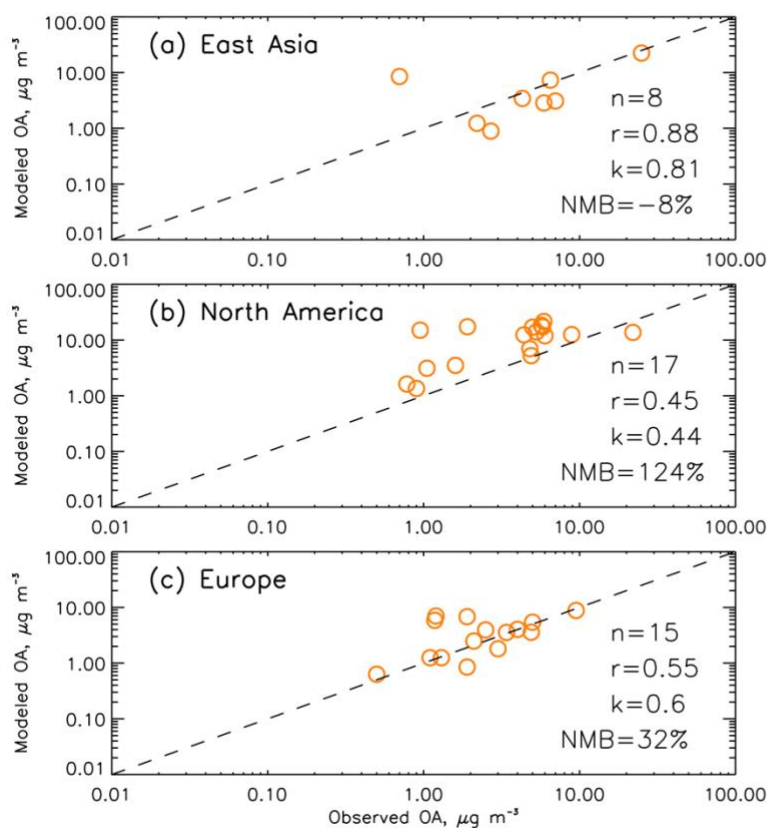
885

886 **Figure 1.** Comparisons of observational and model simulated annual mean surface BC
 887 concentrations from (a) India, (b) China, (3) IMPROVE, and (d) EMEP. Urban and rural sites are
 888 shown in orange circles and blue triangles for each region. For each panel, the total number of
 889 observational sites (n), model-to-observation regression slopes (k), correlation coefficient (r) and
 890 NMB values are included. The dashed line in each panel represents the 1:1 ratio.

891

892

893

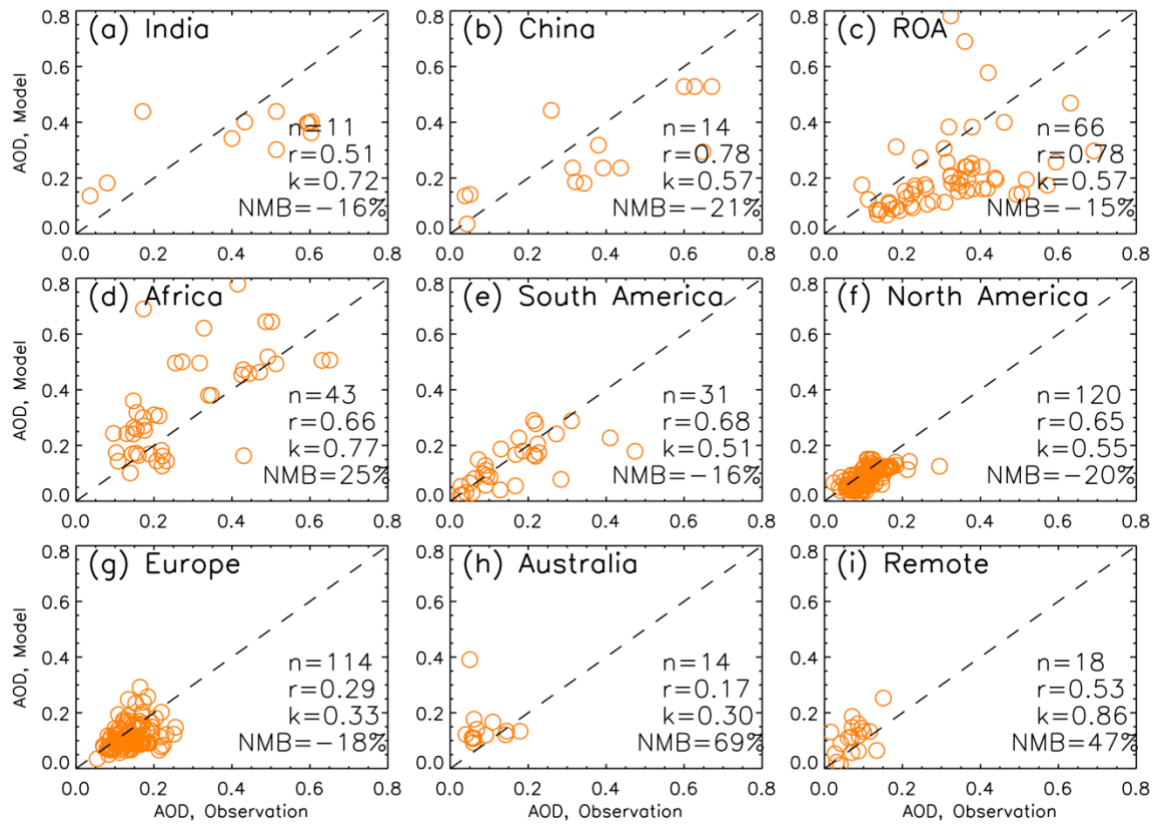


894

895 **Figure 2.** Comparisons of observational and model simulated surface OA concentrations from (a)
 896 East Asia, (b) North America, and (3) Europe. For each panel, the total number of observational
 897 sites (n), model-to-observation regression slopes (k), correlation coefficient (r) and NMB values
 898 are included. The dashed line in each panel represents the 1:1 ratio.

899

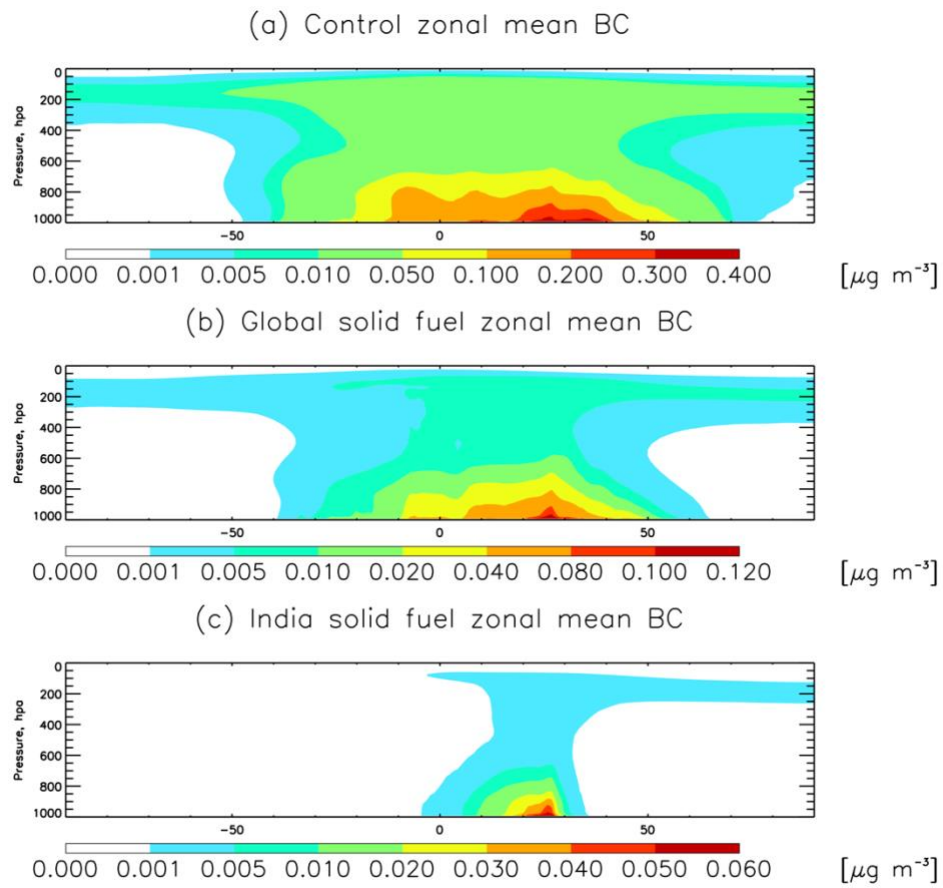
900



901

902 **Figure 3.** Scatter plots of AOD between model simulation and observations over (a) India, (b)
 903 China, (c) Rest of Asia (ROA), excluding China and India, (d) Africa, (e) South America, (f) North
 904 America, (g) Europe, (h) Australia and (i) Remote. For each panel, the total number of
 905 observational sites (n), model-to-observation regression slopes (k), correlation coefficient (r) and
 906 NMB are included.

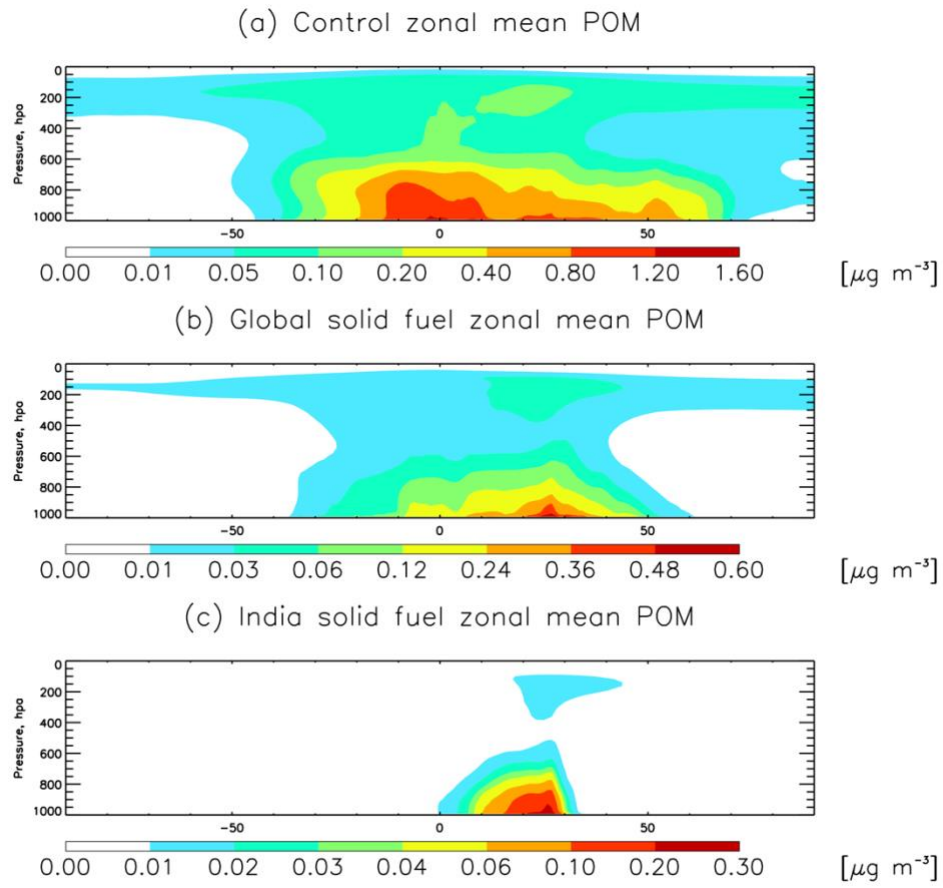
907

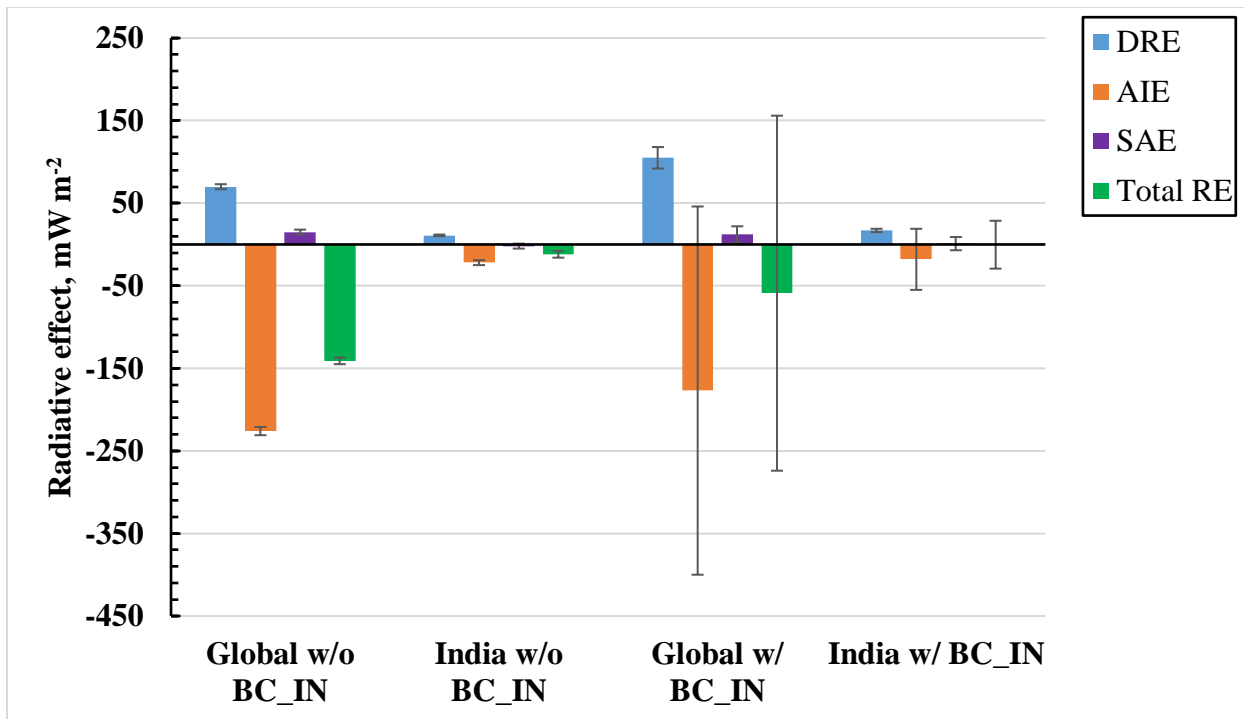


908

909 **Figure 4.** Annual zonal mean BC concentrations from (a) the BASE simulation, (b) the global and
 910 (c) India solid fuel cookstove emissions. BC concentrations are calculated under standard
 911 temperature and pressure conditions (273 K, 1 atm).

912





916

917 **Figure 6.** Radiative effect (RE) for global and Indian solid fuel cookstove aerosol emissions with
 918 BC not serving as IN (w/o BC_IN) and BC as IN (BC_IN), with DRE (blue), AIE (orange), SAE
 919 (purple) and total RE (green). Error bars represent one standard deviation for each RE. For BC as
 920 IN, standard deviations of RE are solely based on the choices of maximum freezing efficiency of
 921 BC as 0.01, 0.05 and 0.1 respectively.

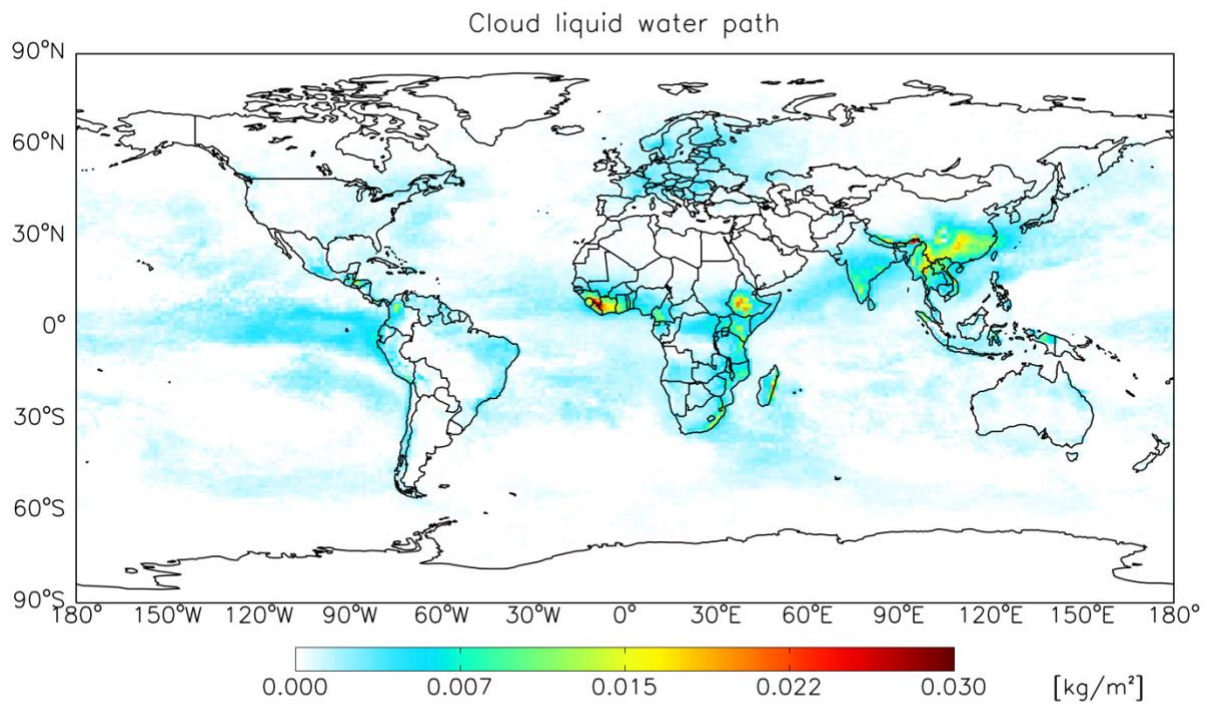
922

923

924

925

926



927

928 **Figure 7.** Global vertically-integrated cloud liquid water path from the global solid fuel cookstove
929 emissions.

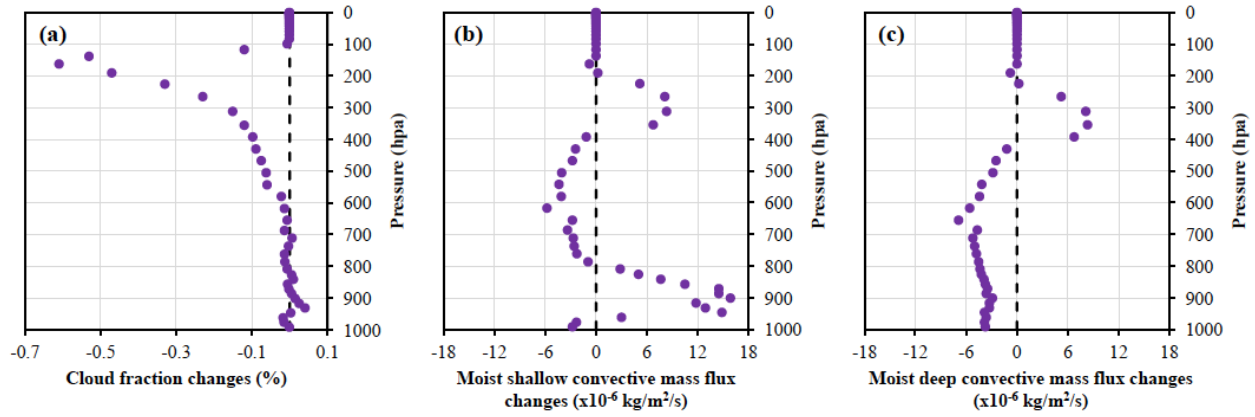
930

931

932

933

934



935

936 **Figure 8.** Changes in vertical cloud fractions (a), shallow (b) and deep (c) convective mass flux
 937 within the India and Indian Ocean domain from global solid fuel cookstove emissions.

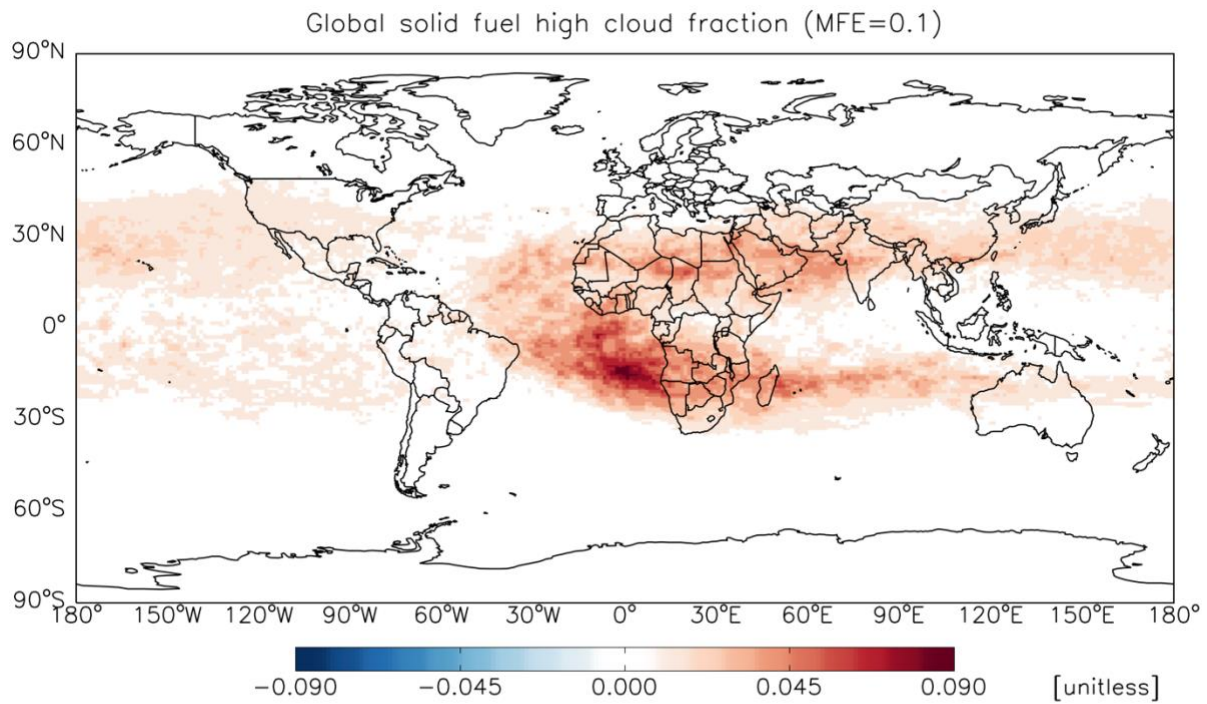
938

939

940

941

942



943

944 **Figure 9.** Global distribution of high cloud fraction due to solid fuel cookstove aerosol emissions
945 with BC as IN and MFE=0.1.

946

947

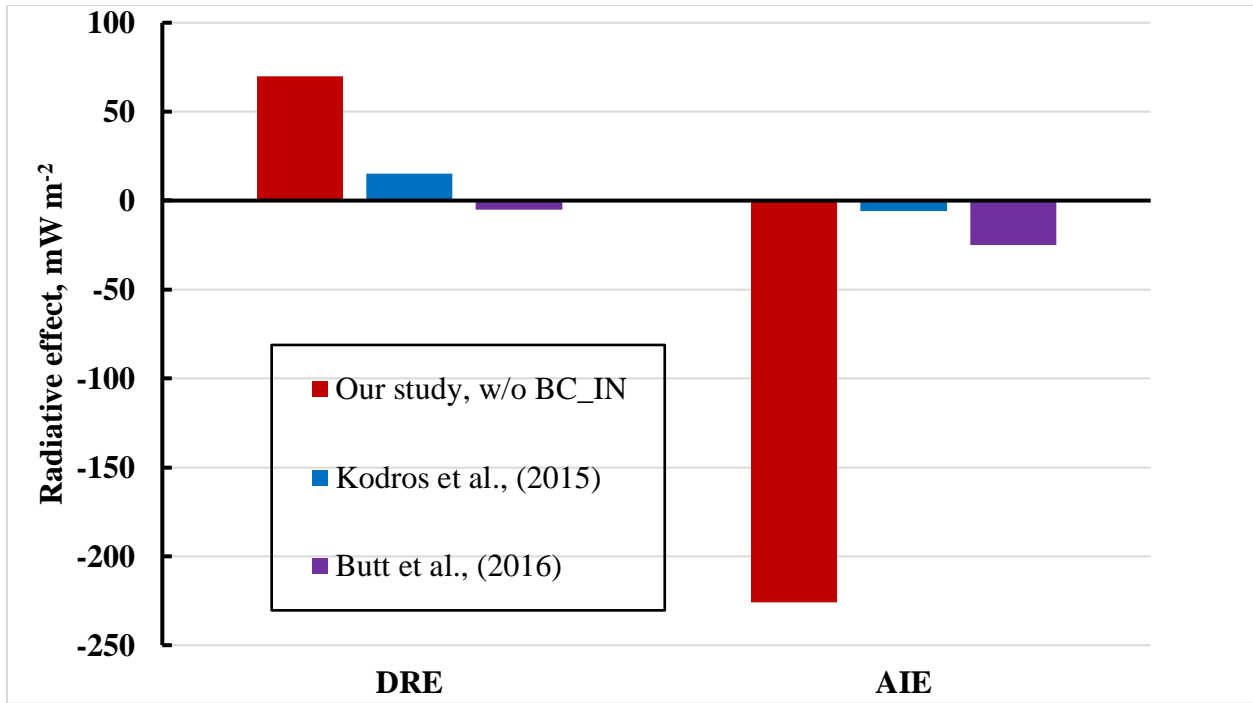
948

949

950

951

952



953

954

955 **Figure 10.** Comparisons of DRE (left) and AIE (right) radiative effects from global solid fuel
 956 cookstove emissions in our control simulation with Kodros et al. (2015) and Butt et al. (2016).

957

958